Allele-specific collateral and fitness effects determine the dynamics of fluoroquinolone-resistance evolution

Apostolos Liakopoulos[a,1*], Linda B. S. Aulin[b,1], Matteo Buffoni[a], J. G. Coen van Hasselt[b], Daniel E. Rozen[a*]

[a]Department of Microbial Biotechnology and Health, Institute of Biology, Leiden University, Leiden, The Netherlands

[b]Leiden Academic Centre for Drug Research, Leiden University, Leiden, The Netherlands.

[1]These authors contributed equally.

*Corresponding authors:

Apostolos Liakopoulos

Daniel E. Rozen

Department of Microbial Biotechnology and Health

Institute of Biology, University of Leiden

Sylviusweg 72, 2333 BE, Leiden, The Netherlands

Tel: +31 71 527 4754

Email: a.liakopoulos@biology.leidenuniv.nl

d.e.rozen@biology.leidenuniv.nl

Running title: Collateral effects in *Streptococcus pneumoniae*

Abstract

Collateral sensitivity (CS), which arises when resistance to one antibiotic increases sensitivity towards other antibiotics, offers novel treatment opportunities to constrain or reverse the evolution of antibiotic resistance. The applicability of CS-informed treatments remains uncertain, in part because we lack an understanding of the generality of CS effects for different resistance mutations, singly or in combination. Here we address this issue in the Gram-positive pathogen *S. pneumoniae* by quantifying collateral and fitness effects of a series of clinically relevant first-step (gyrA or parC) mutations, and their combinations, that confer resistance to fluoroquinolones. We integrated these results in a mathematical model which allowed us to evaluate how different *in silico* combination treatments impact the dynamics of resistance evolution. We identified common and conserved CS effects of different gyrA and parC mutations; however, the spectrum of collateral effects was unique for each mutation or mutation pair. This indicated that mutation identity, even different mutations to the same amino acid, can impact the evolutionary dynamics of resistance evolution during monotreatment and combination treatment. In addition, we observed that epistatic effects between gyrA and parC mutations strongly alter the strength of collateral effects against different antibiotics. Our model simulations, which included the experimentally derived antibiotic susceptibilities and fitness effects, and antibiotic specific pharmacodynamics, revealed that both collateral and fitness effects impact the population dynamics of resistance evolution. Overall, we provide evidence that the gene, mutational identity, and interactions between resistance mutations can have a pronounced impact on collateral effects to different antibiotics and suggest that these need to be considered in models examining CS-based therapies.

Significance

A promising strategy to overcome the evolution of antibiotic resistant bacteria is to use collateral sensitivity-informed antibiotic treatments that rely on cycling or mixing of antibiotics, such that that resistance towards one antibiotic confers increased sensitivity to the other. Here, focusing on multi-step fluoroquinolone resistance in *Streptococcus pneumoniae*, we show that antibiotic-resistance induces diverse collateral responses, whose magnitude and direction are determined by mutation identity and epistasis between resistance mutations. Using mathematical simulations, we show that these effects can be exploited via combination treatment regimens to suppress the *de novo* emergence of resistance during treatment.

Keywords: antibiotic resistance, collateral sensitivity, population dynamics, epistasis, pharmacokinetics/pharmacodynamics, *Streptococcus pneumoniae*

Introduction

Antibiotics are a cornerstone of the prevention and treatment of bacterial infections; however, their efficacy is rapidly declining due to the emergence and spread of antibiotic resistance (1). Advances in antibiotic discovery and design have not kept pace with resistance evolution (2), necessitating new experimentally validated treatment strategies (3). Selection inversion, a strategy that aims to circumvent the emergence and dissemination of antibiotic resistance by combining existing antibiotics based on their physiological and/or evolutionary interactions, has recently gained prominence (4). Among these, collateral sensitivity-informed strategies are particularly promising (5).

Collateral sensitivity (CS) occurs when mutations conferring resistance to one antibiotic concomitantly increase sensitivity towards other antibiotics in the same or different functional class (6). Because of this effective trade-off, bacteria treated with a pair of drugs exhibiting reciprocal CS are unable to simultaneously evolve resistance to both agents (4). Recent studies have examined the frequency and mechanisms of CS, although these have been largely restricted to laboratory strains of a small number of bacterial species (5, 7–13). In addition, none of these studies have examined if collateral effects are conserved for different clinically circulating resistance mutations to the same antibiotics. This is especially relevant given that resistance to any given antibiotic can arise from mutations in different genes or at different sites within a gene (14). Because these mutations cause distinct phenotypic effects, both with respect to changes in MIC and bacterial fitness (15), they may also underlie a distinct spectrum of collateral effects, only some of which would be suitable for CS-informed therapies. To address this limitation, we examine collateral

responses to distinct mutations that confer resistance to fluoroquinolones (FQ) in the Gram-positive pathogen *Streptococcus pneumoniae*.

S. pneumoniae invasive infections are responsible for the most deaths among vaccine-preventable diseases globally (16). Fluoroquinolones are a mainstay of treatment against invasive pneumococcal disease (17), but successful FQ treatment is threatened by the emergence of FQ-resistant strains, which have been reported to be as high as 10.5% (18). *De novo* FQ-resistance in *S. pneumoniae* arises predominantly via the stepwise accumulation of chromosomal mutations in the quinolone resistance-determining regions (QRDRs) of the DNA gyrase (*gyrA*) and/or topoisomerase IV (*parC*) genes (18). Mutations in either *gyrA* or *parC* gene result in low-level FQ-resistance, whereas mutations in both genes result epistatically in high-level resistance, often affecting multiple agents within the class (17, 19). Different mutations in QRDR regions, in pneumococci and other species, have varying impacts on FQ-resistance and on the fitness of strains carrying them (20, 21), effects that are believed to influence the population frequencies of different mutations during monotreatment (22). If similar phenotypic heterogeneity exists for collateral responses, this could impact the efficacy of CS-based combination therapies and the persistence and spread of FQ-resistance.

Here, we studied collateral effects of FQ-resistance by generating isogenic *S. pneumoniae* mutants via allelic replacement that encode a diverse range of clinically relevant FQ-resistance mutations in *gyrA* and *parC*. These mutants were used to assess how different mutations conferring resistance to the same antibiotic influence the susceptibility to other antibiotics and whether epistasis among these mutations modulates their collateral effects. We then developed and applied a mathematical

model to quantitatively study the population dynamics of resistance evolution during different antibiotic combination treatment regimes.

Results

Extensive and conserved collateral effects to fluoroquinolone resistance

To investigate collateral effects to FQ resistance in *S. pneumoniae*, we generated a panel of 16 isogenic D39 strains harboring mutations in the QRDRs of *gyrA* and/or *parC* by CSP-induced transformation (**Figure 1**). Eight strains carried single amino acid mutations in either gyrA (gx, with x = S81F, S81Y, E85G or E85K) or parC (py, with y = S79F, S79Y, D83N or D83Y) and are hereafter denoted as Mgx and Mpy, respectively. The eight double-mutant combinations of these gyrA and parC mutations are denoted as Mgx::py. All mutants showed decreased susceptibility to ciprofloxacin, where the Mgx::py showed the most pronounced MIC increase (32 - 64 mg/L), followed by Mpy (16 - 32 mg/L), and lastly Mgx (MIC 8 mg/L) (**Figure S1**). The collateral effects of these mutants were assessed against 12 antibiotics belonging to a broad range of classes, including commonly used anti-pneumococcal agents.

Collateral effects were observed in approximately 52% of the possible instances (100 out of 192) against all tested antibiotics (**Figure 2**). Among these, 87% were CS and the remaining 13% CR. For 7 of 12 antibiotics, collateral effects were in the same direction for all mutants (CS), whereas for the remaining antibiotics collateral effects were mixed between CS and CR. All mutants (100%) exhibited CS to gentamicin, 81.3% to clindamycin, 75.0% to tetracycline, 56.3% to trimethoprim/sulfamethoxazole, 43.8% to penicillin and fusidic acid, and only 6.3% to vancomycin.

Single Mgx and Mpy strains exhibited CS to a median of four antibiotics with log-scale fold changes relative to the isogenic WT varying from -0.42 to -1.58, and CR to a median of one antibiotic with fold change of 0.42. Mgx::py double-mutant strains exhibited CS to a median of seven antibiotics with log-scale fold changes relative to the isogenic WT varying from -0.42 to -2 and CR to a median of 0.5 antibiotic with fold changes of 0.42 to 1. Conserved CS effects to gentamicin and clindamycin were pronounced, with a median log-fold decrease in MICs of 1.2 and 1 respectively.

Hierarchical clustering revealed four antibiotic groups for which resistant mutants exhibited similar collateral effects (**Figure S2**); only one of these groups consisted exclusively of functionally similar antibiotics, including the protein synthesis inhibiting antibiotics, gentamicin and clindamycin, confirming that collateral effects cannot be simply predicted based on the antibiotic target. Single and double mutants did not cluster distinctively based on their effects within the five strain clusters that we observed (**Figure S2**); this indicates that many of the collateral effects in double mutants are caused by the first-step mutations, although the magnitude of these effects is altered in the double-mutants, as discussed below.

Between and within locus heterogeneity in collateral effects

FQ-resistance can be caused by non-synonymous mutations at the same or different codon within *gyrA* or *parC*, potentially resulting in distinct collateral effects, as depicted in **Figure 2**. Although Mgx and Mpy strains exhibited largely similar collateral effects, we observed between and within locus heterogeneity in CS effects, even for different mutants at the same amino acid. Different gyrA S81 mutations conferred CS from three (gS81F) to eight (gS81Y) antibiotics and a median fold

decrease of -0.58 in MICs. Similarly, different parC S79 mutations conferred CS from three (pS79Y) to five (pS79F) antibiotics and a median fold decrease ranging from -0.58 (pS79F) to -1 (pS79Y), while parC D83 mutations conferred CS from four (pD83N) to five (pD83Y) antibiotics and a median fold decrease of -0.58. Collateral resistance was limited to one antibiotic for Mgx and two for Mpy mutants, with median fold increase of 0.42 in MICs. GyrA and parC mutations conferred CS effects to respectively six and four antibiotics for at least 50% of the mutants tested (CS_{50}). Interestingly, the heterogeneity between different non-synonymous point mutations at the same codon in collateral effects was not limited to the number or intensity but also the direction of the effects. For instance, gS81F and gS81Y mutations conferred CR and CS to linezolid respectively and similarly for gE85G and gE85K mutations to daptomycin. Overall, the heterogeneity in collateral effects of different FQ resistance mutations may jeopardize the generality of CS-informed treatment strategies.

Epistasis shapes collateral effects of double mutations

Mgx and Mpy single-mutant strains showed extensive, yet distinct, collateral effects that are antibiotic-, gene- and mutation-specific. Collateral effects in Mgx::py double-mutant strains (**Figure 2**) appeared to differ from those expected based on their respective single mutations, suggesting that epistatic interactions between QRDR mutations resulted in either lower or higher MIC for the collaterally affected antibiotic than what would be expected from the individual effects of both genes. To study these interactions, we compared the observed changes in CS and CR in double mutants to their expected values given additive interactions between their respective isogenic single mutations.

CS was widespread amongst the double mutants (51 out 57; 89.5%), and the majority of these (42 out of 51; 82.3%) were shaped by epistatic interactions (**Figure 3A**). Almost half of these observed interactions (23 out of 42; 54.8%) were associated with negative epistasis, resulting in a decrease in the MIC for the collaterally sensitive antibiotic, whereas the remainder (19 out of 42; 45.2%) showed positive epistasis, thereby increasing the MIC (although still remaining CS). The magnitude of positive and negative epistatic effects were similar, ranging respectively from -0.17 to -1.58 and 0.42 to 2. Hierarchical clustering on the basis of the observed epistatic interactions revealed two antibiotic clusters for which double mutants exhibit similar trends. One of these clusters consisted exclusively of protein synthesis inhibiting antibiotics (**Figure 3A**), suggesting that negative epistatic interactions between QRDR mutations often lead to the perturbation of bacterial protein synthesis.

Epistasis between gyrA and parC mutations was an important determinant of the magnitude of CS effects for different antibiotics (**Figure 3B**). In particular, we observed a significant positive correlation between epistasis and collateral effects for the majority of the antibiotics, most notably for fusidic acid (effect size = 0.72, R^2 = 0.91, $p < 0.05$), tetracycline (effect size = 0.83, R^2 = 0.65, $p < 0.05$) and erythromycin (effect size, 0.95, R^2 = 0.93, $p < 0.05$). Stronger negative epistatic interactions between gyrA and parC mutations therefore result in stronger CS effects, while positive epistatic effects partially attenuate the CS response. Due to the scarcity of Mgx::py mutants found to exhibit collateral effects for rifampicin and vancomycin, the correlation could not be reliably estimated, and are only shown to indicate the direction of the response (**Figure 3B**).

Antibiotic-resistance linked fitness does not predict collateral effects

All Mgx and Mpy strains, aside from MpS79F, had significantly reduced growth rates compared to the WT strain (**Figure 4A**). Mgx::py strains exhibited the lowest mean relative growth rate (0.56; with a range between 0.29 - 0.74), followed by Mgx (0.60; 0.41 - 0.77) and lastly Mpy (0.85; 0.39 - 1.47) strains. Significant between-gene differences in relative growth rate and therefore fitness was observed between Mgx and Mpy, as well as between Mpy and Mgx::py strains (**Figure 4B**). Significant within-gene differences were observed in both Mgx (MgS81F and MgE85K) and Mpy (MpS79F and MpD83N, MpS79F and MpD83Y, MpS79Y and MpS79F), but not in Mgx::py (**Figure 4A**). Consistent with the strong epistasis for collateral effects, we observed significant interactions between QRDR mutations for fitness (**Figure S3**). Specifically, apart from the Mgx::py strains carrying the pS79F, the fitness of all double mutants was shaped by positive epistasis between gyrA and parC mutations, resulting in higher growth rates and therefore smaller fitness costs of resistance than expected (**Figure S4A**). Our analysis indicated that there was no clear overall correlation between the fitness of the mutants and their collateral effects (**Figure S4B**), suggesting that the fitness costs of resistance have only a limited impact on observed CS effects overall. However, this contribution is heterogeneous and antibiotic-dependent. So while increasing relative growth rates were associated with higher CS effects for tetracycline and gentamycin, decreasing relative growth rates were associated with higher CS effects for chloramphenicol, daptomycin, penicillin, and trimethoprim/sulfamethoxazole.

Combination treatment with clinical dosing regimens suppresses *de novo* antibiotic-resistance development

Given that the different resistance mutations induced distinctly different collateral effects and fitness in our experiments, we first assessed the *de novo* emergence and fixation of FQ-resistant mutants under a clinical dosing schedule for ciprofloxacin monotreatment (500 mg b.i.d., C_{ss} 1.39 mg/L), and in combination with erythromycin (600 mg b.i.d., C_{ss} 0.48 mg/L), linezolid (600 mg b.i.d, C_{ss} 7.33 mg/L), and penicillin (3000 mg b.i.d., C_{ss} 6.95 mg/L). To this end, we developed a mathematical model to study the impact of collateral and fitness effects on treatment outcomes (**Figure 5B**). The model incorporated experimentally derived antibiotic MICs, collateral and fitness effects, and antibiotic-specific pharmacodynamic relationships (details and estimated parameters can be found in Appendix 2). For different simulation scenarios we then computed the probability of resistance evolution for each of the eight mutational trajectories shown in **Figure 5**. Each mutational trajectory comprised one double-mutant and its corresponding single mutant strains. Resistance was defined as the emergence and fixation of the Mgx, Mpy and/or Mgx::py subpopulation.

Our simulations of clinical ciprofloxacin dosing schedules, where C_{ss} equates to 0.9-fold of WT MIC (1.5 mg/L), revealed that monotreatment was ineffective and promoted resistance evolution (**Figure 6A-B**) for all mutational trajectories due to the emergence of single step FQ-resistant mutants (Mgx and/or Mpy). However, adding a second drug effectively suppressed the fixation for any FQ-resistant subpopulation (**Figure 6C**). Specifically, linezolid (1.5 mg/L, 4.9 x WT MIC) and penicillin (0.012 mg/L, 594 x WT MIC) treatments resulted in 0% probability of resistance, whereas erythromycin treatment (0.19 mg/L, 2.6 x WT MIC) had less than 3% resistance evolution. Overall our findings support the idea that antibiotic combinations minimize the risk of *de novo* antibiotic-resistance evolution.

Probability of *de novo* resistance evolution varies between mutational trajectories

Next, to examine the effects of CS-informed treatments that would allow for lower antibiotic concentrations due to collateral effects, we simulated combination treatments with C_{ss} ranging from 0.25 to 2 x MIC (*i.e.* -2 to 1 log2 MIC) of the WT population. Our simulations indicated that suppression of FQ-resistance was primarily observed for dosing schedules with C_{ss} equal to or larger than the MIC of the WT population (**Figure 7A**). Concentrations greater than the WT MIC of either the ciprofloxacin or any of the combined antibiotics (erythromycin, linezolid, and penicillin) resulted in complete bacterial eradication, despite simulating lower concentrations of the second antibiotic than with the clinical dosing regimen.

In addition, our simulations showed that the population dynamics and treatment outcomes for ciprofloxacin mono- and combination treatments with C_{ss} mostly below the MIC of the WT population varied both within and between antibiotic treatments and mutational trajectories (**Figure 7**, **Figure S5-6**, **Table S6**). In particular, the fixation in the population of each specific Mgx and Mpy strain varied between mutational trajectories due to competition between these two arising clonal lineages. The fixation of Mgx and therefore resistance evolution largely differed for the same treatment depending on the concurrent Mpy strain, but not vice versa. This is especially evident when comparing our eight different mutational trajectories treated with 0.5 x MIC for both ciprofloxacin and linezolid (**Figure 7B**), where treatment resulted in high probabilities of fixation for at least one FQ-resistant subpopulation (> 99.3 %), most often the Mpy. The probability of fixation for different Mgx strains varied across mutational trajectories, *e.g.* whereas the

probability of fixation of MgS81F was 0% when MpS79F was the concurrent mutant (Mutational trajectory 4), it rose to 100% when MpD83N was the concurrent mutant (Mutational trajectory 1). Overall, these findings suggest that mutant specific collateral and fitness effects have an impact on the dynamics of FQ-resistance evolution.

Collateral and fitness effects determine the outcome of antibiotic combination treatments

The heterogeneous fixation of individual mutants observed in antibiotic treatments with C_{ss} at sub-MIC concentrations, depicted in **Figure 7**, prompted us to assess the impact of collateral and fitness effects on this phenomenon. Therefore, we simulated four scenarios for all mutational trajectories treated with ciprofloxacin (0.5 x MIC) and penicillin (0.5 x MIC), where the strength of selection pressure exerted from the two antibiotics was similar (**Figure 8**). The first scenario of the model removed the experimentally derived collateral and fitness effects, while the remaining simulations included either the collateral or the fitness effect, or both.

In the absence of fitness differences between resistant strains and CS effects, the ciprofloxacin-penicillin combination treatment was ineffective, resulting in approximately 88% FQ-resistance for all mutational trajectories due to the emergence and fixation of both Mgx and Mpy. However, the probability of resistance varied greatly among the different mutational trajectories and for specific mutants when including fitness effects, especially for mutational trajectories that include MgS81F (1, 2, 4, and 7). In particular, the probability of emergence and fixation of the MgS81F strain ranged from 0 % when paired with the higher-fitness MpS79F strain (Mutational trajectory 4) to 100% when paired with the lower-fitness MpD83N

(Mutational trajectory 1), highlighting the importance of clonal competition in resistance evolution.

The simulations informed solely by the experimentally derived collateral effects showed a decrease in the emergence and fixation of all Mgx (Mutational trajectories 3, 5 and 8) and Mpy (Mutational trajectory 1) strains exhibiting CS towards penicillin from 100% to 0% in our eight defined mutational trajectories, highlighting the potential of CS-informed antibiotic combinations. Finally, we observed the same decreased probability of the fixation of FQ-resistant mutants when the model included both collateral and fitness effects. However, all mutants exhibiting CS to penicillin were also associated with low relative growth rates, thus limiting our ability to disentangle the role of collateral and fitness effects. We observed a similar impact of both fitness and collateral effects when we simulated a second antibiotic combination treatment (*i.e.* 1 x MIC ciprofloxacin and 0.25 x MIC linezolid; **Figure S7**). Overall, our findings suggest that both collateral and fitness effects can impact resistance evolution.

Discussion

In this study, we determined the collateral and fitness effects of clinically relevant FQ-resistance mutations on *S. pneumoniae* susceptibility to a wide range of antibiotics. Although the resistant strains varied in their responses, we observed extensive and conserved CS towards the majority of the antibiotics tested, consistent with earlier results derived from laboratory-evolved strains of *Enterococcus faecalis* (7), *Pseudomonas aeruginosa* (8, 9) and *Escherichia coli* (5, 13). FQ-resistance mutations in *gyrA* and *parC* result in three-dimensional structural changes of the DNA gyrase and the topoisomerase IV that are associated with the modification of

DNA topology (23) and subsequently the global reprogramming of gene expression (24, 25), which in turn leads to collateral effects in *Salmonella enterica* serovar Typhimurium (26). Hence, we hypothesize that this gene expression reprogramming is responsible for the observed extensive collateral effects in *S. pneumoniae* as well, although this remains to be elucidated.

CS was much more predominant than CR and the magnitude of both effects were moderate, with the exception of the strong CS towards gentamicin and clindamycin. In addition, we observed highly conserved CS towards several agents used for the treatment of *S. pneumoniae* infections (17), suggesting that CS-informed combination treatment may be promising for limiting the evolution of FQ-resistance. Interestingly, most mutants exhibited CS towards tetracycline and chloramphenicol, consistent with earlier findings based on *E. faecalis* (7) but not on *E. coli* (5). Similarly with *E. coli* (13) and in contrast with *P. aeruginosa* (8), we observed conserved CS towards gentamicin. These variations highlight that antibiotic-resistance in different species- and/or genetic backgrounds can have distinct collateral effects, necessitating a more systematic preclinical mapping of the pathogen-antibiotic combinations to access the generality and applicability of CS-informed combination therapies.

Our results contrast with an earlier study in *E. coli* suggesting that antibiotic-resistance associated fitness costs are amongst the main contributors to collateral effects (13). Instead, collateral effects and their magnitude seemed to vary depending on the position of the amino acid substitution and the substitution itself in gyrA and parC for the low-level single-step resistant mutants. In high-level double-mutant resistant strains these effects depended on the epistatic interactions between the encoded gyrA and parC mutations. In particular, negative epistasis between FQ-

resistance mutations resulted in greater susceptibility than expected from the individual effects of both genes, especially for antibiotics belonging to protein synthesis inhibitor classes, highlighting the potential of the latter for CS-informed combination treatments of high-level FQ-resistant *S. pneumoniae* strains. As yet, the mechanisms driving the different epistatic interactions between mutations and across antibiotics observed here remain unknown.

Mathematical models are important tools to understand the effects of antibiotic treatments focusing on selection inversion strategies (27). Using a modelling approach, we combined our experimental findings on CS and fitness costs, with antibiotic pharmacokinetics and pharmacodynamics in order to understand multistep resistance evolution in *S. pneumoniae* under different treatment conditions. For the simulated mutational trajectories under treatment combinations with ciprofloxacin-penicillin (0.5 x MIC - 0.5 x MIC) and ciprofloxacin-linezolid (1 x MIC - 0.25 x MIC), we showed that both CS and fitness had an impact on resistance evolution. The impact of the collateral effect was most pronounced for treatments with antibiotic concentrations around the MIC of the WT, possibly due to the limited magnitude of the collateral effects observed for the tested antibiotics. Simulating clinical treatments, which generally resulted in plasma concentration greater than MIC (0.9-594 x WT MIC), showed a clear benefit of erythromycin, penicillin, and linezolid combination therapies over ciprofloxacin monotreatment. However, this benefit is unlikely to be driven by collateral effects, but rather the intrinsically increased bacterial killing associated with the additive effect of the second antibiotic. This conclusion is supported by the lack of variability of resistance evolution between the different mutational trajectories.

Translating a complex system into a simplified model requires a number of assumptions, which should be taken into consideration when interpreting model simulation results. Our pharmacodynamic model includes parameters derived from early phase data from several *in vitro* time-kill literature studies, using different *S. pneumoniae* strains (28–33). This approach allowed us to obtain typical effect parameters of *S. pneumoniae* rather than strain specific effects. We assumed that the early phase data represent the antibiotic-mediated killing of one homogenous population, thus ignoring the possibility of the observed killing rate being affected by the growth of less susceptible subpopulations. Furthermore, we assumed that there were neither pharmacokinetic nor pharmacodynamic interactions between the antibiotics tested, thus ignoring possible synergistic or antagonistic effects of combination treatments. Only FQ-resistance was considered in the model while resistance evolution and possible collateral effects of the second antibiotic was ignored. The model could be further expanded to include such information, thus allowing us to investigate the impact of reciprocal versus non-reciprocal collateral effects, as well as sequential treatment regimens to exploit these reciprocal effects.

In conclusion, we showed that the FQ-resistance mutation- and gene- identity, as well as the interactions between these mutations can have a pronounced impact on collateral effects to different antibiotics in *S. pneumoniae* and could be used to inform combination treatment in order to suppress the *de novo* emergence of resistance. However, our findings under antibiotic mixing regimes highlighted that multistep resistance evolution for mutational trajectories leading to high-level FQ-resistance cannot be predicted solely based on collateral effects. Instead, resistance evolution is affected by an interaction between strain fitness and collateral effects, both of which need to be considered for selection inversion strategies. In addition, our results

highlight the importance of estimating CS for different resistance mutations to the same antibiotic; just as different mutations impart different fitness costs, so too can they drive distinct collateral responses, in turn affecting their probability of fixation during combination treatments.

Material and Methods

Bacterial strains, growth conditions and media

Six FQ-resistant *S. pneumoniae* strains encoding mutated *gyrA* and/or *parC* genes were provided by the CDC Streptococcus Laboratory and used as donors for all subsequent transformations with *S. pneumoniae* D39 strain as the wild-type (WT) recipient strain. *S. pneumoniae* ATCC 49619 was used as a quality control for antimicrobial susceptibility testing. All strains used in this study and their relevant characteristics are listed in **Table S1**. Strains were routinely grown either on tryptic soy agar (BD, New Jersey, USA) supplemented with 0.5% w/v yeast extract (BD, New Jersey, USA) and 5% v/v sheep blood (Sanbio, Uden, The Netherlands) (TSYA) or in tryptic soy broth (BD, New Jersey, USA) supplemented with 0.5% w/v yeast extract (TSYB) at 37°C under 5% CO_2 for 18-24 h, unless otherwise mentioned. The 14 antibiotics used in this study were prepared from powder stock according to manufacturers' recommendations, stored at -20 ^{o}C or -80 ^{o}C and are listed in **Table S2**.

Construction of fluoroquinolone-resistant mutants

Amplified fragments from genomic DNA of the FQ-resistant *S. pneumoniae* strains encoding each of the non-wild type *gyrA* or *parC* gene allele and at least 1 Kb of its flanking regions necessary for the integration by double crossover were used to

transform the *S. pneumoniae* D39 strain. All the primer sequences used in this study are listed in **Table S3**. Transformation was performed using a saturating concentration of 1 μg/ ml of amplified DNA and 0.1 μg/ ml synthetic competence stimulating peptide 1, CSP-1 (GenScript, New Jersey, USA), as previously described (34). Putative first-step *gyrA* (Mgx) and *parC* (Mpy) mutants were selected on TSYA plates supplemented with 0.5 mg/L sparfloxacin (Santa Cruz Biotechnology, Texas, USA) or 4 mg/L ciprofloxacin (Acros Organics, New Jersey, USA), respectively. Double QRDR (Mgx::py) mutants were generated by transforming sequentially with the *parC* and then *gyrA* non-WT alleles and selecting on TSYA plates supplemented with 12 mg/L ciprofloxacin (Acros Organics, New Jersey, USA). *GyrA* and *parC* allelic replacements in the transformants were confirmed by PCR and Sanger sequencing.

Antimicrobial susceptibility testing

Minimum inhibitory concentrations (MICs) of all isogenic strains for 12 clinically relevant antibiotics and ciprofloxacin (**Table S2**) were determined in triplicate by broth microdilution according to European Committee on Antimicrobial Susceptibility Testing (EUCAST; http://www.eucast.org) and ISO 20776-1:2006 guidelines with two minor modifications. A 1.5-fold testing scale was used to include the standard two-fold antibiotic concentrations and their median values and the cation-adjusted Mueller-Hinton broth (BD, New Jersey, USA) was supplemented with 100 U of catalase (Worthington Biochemical Corporation, New Jersey, USA) instead of 5% lysed horse blood. The lowest antibiotic concentration where no turbidity was observed was scored as the MIC.

Collateral effect and epistasis determination

Collateral effects were determined as the decrease (CS) or increase (collateral resistance, CR) in the MIC of each mutant relative to the isogenic WT D39 strain, and their magnitude as the log2-scaled fold change in the MICs between each mutant and the WT D39 strain (Equation 1), as previously described (7).

$$CE_M = log2\left(\frac{MIC_M}{MIC_{WT}}\right) \qquad \text{Equation 1}$$

Where CE_M represents the collateral effect of a mutant (Mgx, Mpy, or Mgx::py), MIC_M its corresponding MIC and MIC_{WT} the MIC of the D39 WT strain.

The conservation of the collateral effects was assessed based on the CS_{50} and CR_{50} thresholds, defined respectively as CS and CR effects occurring in more than 50% of the mutants tested (13). The expected relative collateral effects of the double mutants were calculated by the individual effects of each single mutation based on the additive model on a log-scale (Equation 2), and any deviation from this was considered as epistasis (35). Negative epistasis denotes a lower MIC (more susceptible) of the double mutant than expected for the collaterally affected antibiotic, while positive epistasis denotes a higher MIC (less susceptible) than expected.

$$Epistasis = CE_{Mgx::py} - \left(CE_{Mgx} + CE_{Mpy}\right) \qquad \text{Equation 2}$$

Where $CE_{Mgx::py}$, CE_{Mgx}, and CE_{Mgpy} represent the collateral effects of the Mgx::py, Mgx, and Mpy, respectively.

Growth rate measurements

The *in vitro* fitness of the WT and each mutant was determined in triplicate using the Malthusian growth model (36). Bacterial inocula of ~10^8 CFU/ ml were diluted 100-fold into 3 ml of fresh pre-warmed TSYB medium. 200 µl of each diluted culture was loaded in wells of a 100-well honeycomb plate and incubated at 37 °C. Subsequently, the optical density at 600 nm was measured hourly using a Bioscreen C Reader (Thermo Scientific, Breda, The Netherlands), with 5 s of shaking before reads. Growth rates were calculated based on the slope of the line that fitted points displaying log-linear growth. Relative growth rates were calculated by dividing the generation time of each D39 mutant by that of the mean growth rate of the WT D39 strain.

Statistical analysis

Statistical analyses were performed using R (version 3.6.3). We performed hierarchical clustering to identify relationships between strains, and between antibiotics, relating to collateral effects and epistasis using the complete linkage method within the stats R package. We evaluated between and within group differences in mean relative growth rate with a one-way ANOVA and a post-hoc Tukey pairwise comparison with multiple correction when significant differences were identified ($\alpha = 0.05$). To evaluate the relationship between mean relative growth rate and collateral effects we computed the Kendall correlation coefficient for each antibiotic. We quantified the relationship between collateral effect size and epistasis using linear regression, where the effect size reflects the strength of the relationship. The statistical significance of the correlation was evaluated comparing the full slope model to a reduced intercept model with a significance level of 0.05.

Mathematical modeling

We performed mathematical modeling of bacterial growth dynamics to evaluate the effect of different FQ mono- and combination-treatments (antibiotic mixing) for eight different mutational trajectories towards double-mutant strains on treatment outcomes and the probability of resistance. The model included clinical antibiotic pharmacokinetics of antibiotics used in the treatment schedule, bacterial growth rates, antibiotic-mediated killing, collateral effects, and resistance development through stepwise mutations (**Figure 5**). The treatment simulations were conducted for ciprofloxacin monotreatment and in combination with erythromycin, linezolid, and penicillin, which were chosen because of the availability of literature derived experimental data (28–33) needed for the estimation of pharmacodynamic parameters. We incorporated the experimentally measured relative fitness and collateral effects observed for the strains designed in this study.

The bacterial model was comprised of a four-state stochastic hybrid ordinary differential equation (ODE) model (details can be found in Appendix 1), where each state represents a bacterial subpopulation. Included *S. pneumoniae* subpopulations were the FQ-sensitive D39 wild-type (WT; $gyrA_{wt}$::$parC_{wt}$), the resistant *gyrA* mutant (Mgx; $gyrA_{x}$::$parC_{wt}$), the resistant *parC* mutant (Mpy; $gyrA_{wt:}$:$parC_{y}$), and the resistant *gyrA* and *parC* double mutant (Mgx::py; $gyrA_{x}$::$parC_{y}$). Evolution of *de novo* resistance occurred in a stepwise manner with either a first step *gyrA* or *parC* mutation, followed by a second step mutation resulting in the *gyrA* and *parC* double mutant. The mutation events were modelled by a stochastic process. This process was based on a binomial distribution with a mutation probability equal to the *gyrA* and *parC* mutation frequency (μ) (37) and was identically implemented for each state transition.

Each bacterial state (z) included a logistic growth model for which the state-specific maximal growth rate ($k_{G,z}$) was a composite parameter of the literature derived growth rate of D39 (38) and our experimental growth rate ratio between mutant and WT. The systems growth capacity limitation parameter (B_{max}) and the bacterial concentration at the start of the infection were obtained from an *in vivo* model of bacteraemia (39). The volume available for infection represented a human blood volume (40). All system specific parameters are stated in **Table S4**.

Antibiotic-mediated killing was implemented according to a previously described model (41) where the effect of the ith antibiotic on bacterial state z ($E_{AB_i,z}$) related to the unbound concentration ($C_{AB,i}$) according to Equation 3. Drug effects were assumed to be additive and the total drug effect for each state z ($E_{AB,z}$) was implemented according to Equation 4.

$$E_{AB_i,z} = \frac{(G_{max} - G_{min,\,AB_i}) \times \left(\frac{C_{AB,i}}{MIC_{AB_i,z}}\right)^{hill_{AB_i}}}{\left(\frac{C_{AB_i}}{MIC_{AB_i,z}}\right)^{hill_{AB_i}} - \frac{G_{min,\,AB_i}}{G_{max}}} \qquad \text{Equation 3}$$

Where $G_{min,\,AB_i} = G_{max} - E_{max,\,AB_i}$, $G_{max} = 1$, with $E_{max,\,AB_i}$ representing the maximal killing effect, $hill_{AB_i}$ being the shape factor of the concentration-effect relationship, and $MIC_{AB_i,\,z}$ being the state specific MIC.

$$E_{AB,z} = 1 - \left(E_{AB_1,z} + E_{AB_2,z}\right) \qquad \text{Equation 4}$$

Pharmacodynamic model parameter values were obtained by fitting the model to digitized early phase *S. pneumoniae* experimental *in vitro* time-kill data using the

nlmixr package (version 1.1.1-7) within the statistical software R (version 3.6.3). Growth in the absence of antibiotic and antibiotic mediated bacterial killing were modelled sequentially. Initially, bacterial maximal growth rates were obtained by fitting an exponential growth model for all the antibiotic-free growth data. A log-normal random effect was included on maximal growth rate to account for between experiment variability. The estimated individual maximal growth rates were included as a covariate in the subsequent fitting of the antibiotic-mediated killing. Separate models were fitted for each antibiotic to obtain the drug specific parameters $E_{max,\,AB_i}$ and $hill_{AB_i}$. Antibiotic-mediated killing was incorporated separately for each antibiotic on each individual bacterial state with the corresponding experimentally determined MICs ($MIC_{AB_i,z}$).

The pharmacodynamic model was linked to a previously published pharmacokinetic model of ciprofloxacin (42) and a pharmacokinetic model of the respective antibiotic selected for combination treatment (**Table S5**). The pharmacokinetic models were used to simulate pharmacokinetic profiles of an individual with a body weight of 70 kg and a creatinine clearance of 75 mL/min/1.73 m^2. The estimate of the 95th percentile of parameters related to clearance and volume were used if the inter-individual variability was reported. The fraction unbound (f_u) was used to obtain the unbound concentration of each antibiotic.

The modeling framework was used to simulate two different treatment scenarios of *S. pneumoniae* bacteraemia: 1) using ciprofloxacin as mono-treatment (500 mg twice daily (b.i.d.)) or in combination with erythromycin (600 mg b.i.d.), linezolid (600 mg b.i.d.), or penicillin (3 g b.i.d.); and 2) using a series of non-clinical treatment scenarios where the average unbound steady state concentration (C_{ss}) of each antibiotic was related to the MIC of the WT (C_{ss} 0.25-2 x MIC). The selection of

the anti-pneumococcal antibiotics included in these treatment scenarios was based on the availability of relevant time-kill data and ciprofloxacin was used as representative agent of the FQ class. Each of the treatment scenarios was simulated 1000 times. The treatment outcomes were evaluated by assessing the probability of failure in eradicating the WT strain and/or the probability of resistance establishment, where failure in WT eradication and resistance establishment were defined respectively as a bacterial density of WT and FQ-resistant mutant strains exceeding 10^4 CFU/ml (initial inoculum) at the end of treatment (two weeks). The framework was used to simulate treatments of eight defined mutational trajectories, each depicting the *de novo* multistep emergence of a particular high-level FQ-resistant double mutant (Mgx::py), with either of its corresponding low-level FQ-resistant single mutants (Mgx or Mpy) as an intermediate step (**Figure 5**).

Acknowledgements

AL and DER were supported through the JPI-EC-AMR (Project 547001002). JGCvH was supported by ZonMW Off Road (Project 451001033).

References

1. J. O'Neill, Antimicrobial Resistance: Tackling a crisis for the health and wealth of nations. *Rev. Antimicrob. Resist.* (2016).
2. M. S. Butler, D. L. Paterson, Antibiotics in the clinical pipeline in October 2019. *J. Antibiot. (Tokyo).* (2020) https:/doi.org/10.1038/s41429-020-0291-8.
3. K. Bush, *et al.*, Tackling antibiotic resistance. *Nat. Rev. Microbiol.* (2011) https:/doi.org/10.1038/nrmicro2693.
4. M. Baym, L. K. Stone, R. Kishony, Multidrug evolutionary strategies to

reverse antibiotic resistance. *Science (80-.).* (2016) https:/doi.org/10.1126/science.aad3292.

5. L. Imamovic, M. O. A. Sommer, Use of collateral sensitivity networks to design drug cycling protocols that avoid resistance development. *Sci. Transl. Med.* (2013) https:/doi.org/10.1126/scitranslmed.3006609.

6. W. Szybalski, V. Bryson, Genetic studies on microbial cross resistance to toxic agents. I. Cross resistance of *Escherichia coli* to fifteen antibiotics. *J. Bacteriol.* (1952).

7. J. Maltas, K. B. Wood, Pervasive and diverse collateral sensitivity profiles inform optimal strategies to limit antibiotic resistance. *PLoS Biol.* (2019) https:/doi.org/10.1371/journal.pbio.3000515.

8. C. Barbosa, *et al.*, Alternative evolutionary paths to bacterial antibiotic resistance cause distinct collateral effects. *Mol. Biol. Evol.* (2017) https:/doi.org/10.1093/molbev/msx158.

9. L. Imamovic, *et al.*, Drug-driven phenotypic convergence supports rational treatment strategies of chronic infections. *Cell* (2018) https:/doi.org/10.1016/j.cell.2017.12.012.

10. G. Jansen, *et al.*, Association between clinical antibiotic resistance and susceptibility of *Pseudomonas* in the cystic fibrosis lung. *Evol. Med. Public Heal.* (2016) https:/doi.org/10.1093/EMPH/EOW016.

11. V. Lázár, *et al.*, Genome-wide analysis captures the determinants of the antibiotic cross-resistance interaction network. *Nat. Commun.* (2014) https:/doi.org/10.1038/ncomms5352.

12. V. Lázár, *et al.*, Bacterial evolution of antibiotic hypersensitivity. *Mol. Syst. Biol.* (2013) https:/doi.org/10.1038/msb.2013.57.

13. N. L. Podnecky, *et al.*, Conserved collateral antibiotic susceptibility networks in diverse clinical strains of *Escherichia coli*. *Nat. Commun.* (2018) https:/doi.org/10.1038/s41467-018-06143-y.

14. J. L. Martinez, F. Baquero, Mutation frequencies and antibiotic resistance. *Antimicrob. Agents Chemother.* (2000) https:/doi.org/10.1128/AAC.44.7.1771-1777.2000.

15. D. Hughes, D. I. Andersson, Evolutionary trajectories to antibiotic resistance. *Annu. Rev. Microbiol.* (2017) https:/doi.org/10.1146/annurev-micro-090816-093813.

16. WHO/UNICEF, Global Immunization Data 2014. *WHO/Unicef Reports* (2015).

17. M. R. Jacobs, Antimicrobial-resistant *Streptococcus pneumoniae*: Trends and management. *Expert Rev. Anti. Infect. Ther.* (2008) https:/doi.org/10.1586/14787210.6.5.619.

18. L. Kim, L. McGee, S. Tomczyk, B. Beall, Biological and epidemiological features of antibiotic-resistant *Streptococcus pneumoniae* in pre- and post-conjugate vaccine eras: A United States perspective. *Clin. Microbiol. Rev.* (2016) https:/doi.org/10.1128/CMR.00058-15.

19. C. Janoir, V. Zeller, M. D. Kitzis, N. J. Moreau, L. Gutmann, High-level fluoroquinolone resistance in *Streptococcus pneumoniae* requires mutations in parC and gyrA. *Antimicrob. Agents Chemother.* (1996).

20. D. E. Rozen, L. McGee, B. R. Levin, K. P. Klugman, Fitness costs of fluoroquinolone resistance in *Streptococcus pneumoniae*. *Antimicrob. Agents Chemother.* (2007) https:/doi.org/10.1128/AAC.01161-06.

21. L. S. Redgrave, S. B. Sutton, M. A. Webber, L. J. V Piddock, Fluoroquinolone

resistance: Mechanisms, impact on bacteria, and role in evolutionary success. *Trends Microbiol.* (2014) https:/doi.org/10.1016/j.tim.2014.04.007.

22. D. L. Huseby, *et al.*, Mutation supply and relative fitness shape the genotypes of ciprofloxacin-resistant *Escherichia coli*. *Mol. Biol. Evol.* (2017) https:/doi.org/10.1093/molbev/msx052.

23. Y. Seol, K. C. Neuman, The dynamic interplay between DNA topoisomerases and DNA topology. *Biophys. Rev.* (2016) https:/doi.org/10.1007/s12551-016-0240-8.

24. E. Marrer, A. T. Satoh, M. M. Johnson, L. J. V. Piddock, M. G. P. Page, Global transcriptome analysis of the responses of a fluoroquinolone-resistant *Streptococcus pneumoniae* mutant and its parent to ciprofloxacin. *Antimicrob. Agents Chemother*. (2006) https:/doi.org/10.1128/AAC.50.1.269-278.2006.

25. A. G. de la Campa, M. J. Ferrándiz, A. J. Martín-Galiano, M. T. García, J. M. Tirado-Vélez, The transcriptome of *Streptococcus pneumoniae* induced by local and global changes in supercoiling. *Front. Microbiol.* (2017) https:/doi.org/10.3389/fmicb.2017.01447.

26. M. A. Webber, *et al.*, Clinically relevant mutant DNA gyrase alters supercoiling, changes the transcriptome, and confers multidrug resistance. *MBio* (2013) https:/doi.org/10.1128/mBio.00273-13.

27. J. G. Coen Van Hasselt, R. Iyengar, Systems pharmacology: Defining the interactions of drug combinations. *Annu. Rev. Pharmacol. Toxicol.* (2019) https:/doi.org/10.1146/annurev-pharmtox-010818-021511.

28. G. A. Pankuch, M. R. Jacobs, P. C. Appelbaum, Study of comparative antipneumococcal activities of penicillin vancomycin by using time-kill methodology. **38**, 2065–2072 (1994).

29. M. A. Visalli, M. R. Jacobs, P. C. Appelbaum, Activity of CP 99,219 (trovafloxacin) compared with ciprofloxacin, sparfloxacin, clinafloxacin, lomefloxacin and cefuroxime against ten penicillin-susceptible and pencillin-resistant pneumococci by time-kill methodology The worldwide incidence of i. **219**, 77–84 (1996).

30. M. D. Huband, *et al.*, *In vitro* and *in vivo* activities of PD 0305970 and PD 0326448, new bacterial gyrase / topoisomerase inhibitors with potent antibacterial activities versus multidrug-resistant gram-positive and fastidious organism groups. **51**, 1191–1201 (2007).

31. N. Frimodt-mller, V. F. Thomsen, The pneumococcus and the mouse-protection test: correlation of *in vitro* and *in vivo* activity for beta-lactam antibiotics, vancomycin, erythromycin and gentamicin. 159–165 (1987).

32. H. M. Alloush, V. Salisbury, R. J. Lewis, A. P. Macgowan, Pharmacodynamics of linezolid in a clinical isolate of *Streptococcus pneumoniae* genetically modified to express lux genes. 511–513 (2003).

33. J. D. Knudsen, N. Frimodt-møller, F. Espersen, A. N. A. G. C. Hemother, Experimental *Streptococcus pneumoniae* infection in mice for studying correlation of in vitro and in vivo activities of penicillin against pneumococci with various susceptibilities to penicillin. **39**, 1253–1258 (1995).

34. B. A. Evans, D. E. Rozen, Significant variation in transformation frequency in Streptococcus pneumoniae. *ISME J.* (2013) https:/doi.org/10.1038/ismej.2012.170.

35. A. Wong, Epistasis and the evolution of antimicrobial resistance. *Front. Microbiol.* (2017) https:/doi.org/10.3389/fmicb.2017.00246.

36. R. E. Lenski, Quantifying fitness and gene stability in microorganisms.

Biotechnology (1991) https:/doi.org/10.1016/b978-0-409-90199-3.50015-2.

37. C. V Gould, *et al.*, Identifying mutator phenotypes among fluoroquinolone-resistant strains of *Streptococcus pneumoniae* using fluctuation analysis. **51**, 3225–3229 (2007).

38. Y. Yu, *et al.*, The virulence of *Streptococcus pneumoniae* partially depends on dprA. **8**, 225–231 (2016).

39. A. Gerlini, *et al.*, The role of host and microbial factors in the pathogenesis of pneumococcal bacteraemia arising from a single bacterial cell bottleneck. **10** (2014).

40. R. Sharma, S. Sharma, Physiology , Blood Volume. *StatPearls* **l**, 6–9 (2020).

41. R. R. Regoes, *et al.*, Pharmacodynamic functions: a multiparameter approach to the design of antibiotic treatment regimens. *Antimicrob. Agents Chemother*. **48**, 3670–3676 (2004).

42. A. Cios, J. Szymura-oleksiak, T. Grodzicki, Population pharmacokinetic analysis of ciprofloxacin in the elderly patients with lower respiratory tract infections. **57**, 107–113 (2014).

43. G. G. Zhanel, *et al.*, The new fluoroquinolones□: A critical review. **10**, 207–238 (1999).

44. A. Kratzer, F. Kees, C. Dorn, Unbound fraction of fluconazole and linezolid in human plasma as determined by ultrafiltration□: Impact of membrane type. *J. Chromatogr. B* **1039**, 74–78 (2016).

45. M. D. Optimization, E. I. Nielsen, O. Cars, L. E. Friberg, Pharmacokinetic / Pharmacodynamic (PK/PD) Indices of Antibiotics predicted by a semimechanistic PKPD model□: a Step toward. **55**, 4619–4630 (2011).

46. T. Sasaki, *et al.*, Population pharmacokinetic and pharmacodynamic analysis of

linezolid and a hematologic side effect, thrombocytopenia, in japanese patients. **55**, 1867–1873 (2011).

47. T. Komatsu, *et al.*, Population pharmacokinetic analysis and dosing regimen optimization of penicillin G in patients with infective endocarditis. *J. Pharm. Heal. Care Sci.*, 2–9 (2016).

Tables

Table S1. *Streptococcus pneumoniae* strains included in this study and their relevant characteristics.

Strains	Relevant characteristic(s)	Source
D39	Encapsulated, Serotype 2, wild-type *gyrA* and *parC*	Laboratory stock
ATCC 49619	Encapsulated, Serotype 19F, wild-type *gyrA* and *parC*	Laboratory stock
SP12	FQ-resistant ($gyrA_{S81Y}$), donors for transformations	CDC
SP35	FQ-resistant ($gyrA_{S81F}$::$parC_{D83Y}$), donors for transformations	CDC
SP47	FQ-resistant ($gyrA_{S81F}$::$parC_{D83N}$), donors for transformations	CDC
SP60	FQ-resistant ($gyrA_{S81F}$::$parC_{S79F}$), donors for transformations	CDC
SP62	FQ-resistant ($gyrA_{E85G}$::$parC_{S79F}$), donors for transformations	CDC
SP95	FQ-resistant ($gyrA_{E85K}$::$parC_{S79Y}$), donors for transformations	CDC
MgS81F	FQ-resistant ($gyrA_{S81F}$::$parC_{WT}$), isogenic D39 transformant	This study
MgS81Y	FQ-resistant ($gyrA_{S81Y}$::$parC_{WT}$), isogenic D39 transformant	This study
MgE85G	FQ-resistant ($gyrA_{E85G}$::$parC_{WT}$), isogenic D39 transformant	This study
MgE85K	FQ-resistant ($gyrA_{E85K}$::$parC_{WT}$), isogenic	This study

	D39 transformant	
MpS79F	FQ-resistant (*gyrA*$_{WT}$::*parC*$_{S79F}$), isogenic D39 transformant	This study
MpS79Y	FQ-resistant (*gyrA*$_{WT}$::*parC*$_{S79Y}$), isogenic D39 transformant	This study
MpD83N	FQ-resistant (*gyrA*$_{WT}$::*parC*$_{D83N}$), isogenic D39 transformant	This study
MpD83Y	FQ-resistant (*gyrA*$_{WT}$::*parC*$_{D83Y}$), isogenic D39 transformant	This study
MgS81F::pS79F	FQ-resistant (*gyrA*$_{S81F}$::*parC*$_{S79F}$), isogenic D39 transformant	This study
MgS81F::pS79Y	FQ-resistant (*gyrA*$_{S81F}$::*parC*$_{S79Y}$), isogenic D39 transformant	This study
MgS81F::pD83N	FQ-resistant (*gyrA*$_{S81F}$::*parC*$_{D83N}$), isogenic D39 transformant	This study
MgS81F::pD83Y	FQ-resistant (*gyrA*$_{S81F}$::*parC*$_{D83Y}$), isogenic D39 transformant	This study
MgS81Y::pS79F	FQ-resistant (*gyrA*$_{S81Y}$::*parC*$_{S79F}$), isogenic D39 transformant	This study
MgS81Y::pS79Y	FQ-resistant (*gyrA*$_{S81Y}$::*parC*$_{S79Y}$), isogenic D39 transformant	This study
MgE85G::pS79F	FQ-resistant (*gyrA*$_{E85G}$::*parC*$_{S79F}$), isogenic D39 transformant	This study
MgE85K::pS79Y	FQ-resistant (*gyrA*$_{E85K}$::*parC*$_{S79Y}$), isogenic D39 transformant	This study

743 **Table S2.** List of antibiotics used in this study and their targets.

Antibiotic Name (Abbreviation)	**Antibiotic class**	**Antibiotic target(s)**	**Supplier**
Chloramphenicol (CHL)	Amphenicol	Protein synthesis (50S)	Sigma-Aldrich
Ciprofloxacin (CIP)	Quinolone	DNA replication (GyrA + ParC)	Acros Organics
Clindamycin (CLI)	Lincosamide	Protein synthesis (50S)	Cayman chemical
Daptomycin (DAP)	Lipopeptide	Cell membrane	Acros Organics
Erythromycin (ERY)	Macrolide	Protein synthesis (50S)	Sigma-Aldrich
Fusidic Acid (FUS)	Fusidane	Protein synthesis (EF-G)	Cayman chemical
Gentamicin (GEN)	Aminoglycosides	Protein synthesis (30S)	Sigma-Aldrich
Linezolid (LNZ)	Oxazolidinone	Protein synthesis (50S)	Cayman chemical
Penicillin (PEN)	β-lactam	Cell wall synthesis (PBPs)	Sigma-Aldrich
Rifampicin (RIF)	Rifamycin	RNA synthesis (rpoB)	GERBU Biotechnik
Sparfloxacin (SPR)	Quinolone	DNA replication (GyrA + ParC)	Cayman chemical

Trimethoprim/sulfamethoxazole (SXT)	Antifolate	Folate synthesis (FolA + FolP)	SERVA/ AG Scientific
Tetracycline (TET)	Tetracycline	Protein synthesis (30S)	Sigma-Aldrich
Vancomycin (VAN)	Glycopeptide	Cell wall synthesis	Carl Roth

Table S3. Oligonucleotides used in this study.

Oligonucleotide	Sequence (5′-3′)	Purpose	Reference
GyrA_1kb_F	TGAAACTAGAATAGTACACC	Amplification of *gyrA* gene and ~ 1Kb flanking regions for allelic replacement.	This study
GyrA_1kb_R	GAACAATTCAATCAATTCAGC	Amplification of *gyrA* gene and ~ 1Kb flanking regions for allelic replacement.	This study
GyrA_3kb_F	AATTATCAACATCGACAAAGG	Amplification of *gyrA* gene and ~ 3Kb flanking regions for allelic replacement.	This study
GyrA_3kb_R	AACACTTGAGAATGAAATTCG	Amplification of *gyrA* gene and ~ 3Kb flanking regions for allelic replacement.	This study
ParC_3kb_F	ACGAATGATAATCAAACTAGC	Amplification of *parC* gene and ~ 3Kb	This study

		flanking regions for allelic replacement.	
ParC_3kb_R	CTAAATTCTGGAATCATTTGC	Amplification of *parC* gene and ~ 3Kb flanking regions for allelic replacement.	This study
gyrA-F-seq	GATACCTGGCTAACTTGATA	Sequencing of *gyrA* gene for confirmation of allelic replacement.	This study
gyrA-R-seq	GATTTTCCCTAGACAACTTC	Sequencing of *gyrA* gene for confirmation of allelic replacement.	This study
parC-F-seq	CCTACTCTACATTCTTTGAAA	Sequencing of *parC* gene for confirmation of allelic replacement.	This study
parC-R-seq	TTACTGTCATATTCCACTCC	Sequencing of *parC* gene for confirmation of allelic replacement.	This study

Table S4. System specific model parameters.

Parameter	**Value**	**Note**	**Reference**
Growth rate ($k_{G,z}$)	0.77 h^{-1} *ratio	Composite parameter of literature D39 natural growth and experimental ratio between WT and mutant	(38)
Mutation rate (μ)	1.4 x 10^{-8}	Literature value for D39 *gyrA* and *parC* mutations. The resistance frequency was calculated as the number of resistant colonies per inoculum (~10^8 cells).	(37)

Maximal capacity (B_{max})	10^8 cfu/ml	Maximal capacity in cfu/ml derived from blood sampling of *in vivo* experiment day 4	(39)
Inoculum	10^4 cfu/ml	Derived from blood sampling of *in vivo* experiment day one	(39)
Infection volume	5 L	Volume of blood to represent bacteraemia	(40)
Bacterial clearance	0.1 h^{-1}	Assumed first order bacterial clearance	

Table S5. Pharmacokinetic model parameters of the antibiotics selected for combination treatment.

Description	**Parameter**	**Ciprofloxacin**	**Erythromycin**	**Linezolid**	**Penicillin**
Central volume	Vc	23.6 L	34.9 L	67.2 L	18.1 L
Clearance	CL	82.9 L/h	22.8 L/h	5.8 L/h	34.3 L/h
Peripheral volume	Vp	NA	20.7 L	NA	NA
Inter-compartmental clearance	Q	NA	16.9 L/h	NA	NA
Unbound fraction	fu	0.79 (43)	0.16	0.815 (44)	0.40
Reference		(42)	(45)	(46)	(47)

All models were either one- or two-compartmental models with first order elimination. NA=Not applicable.

Figure Legends

Figure 1. Overview of experimental workflow. Isogenic mutants of *S. pneumoniae* D39 strain encoding *gyrA* (Mgx, blue), *parC* (Mpy, orange) or double *gyrA*::*parC* (Mgx::py, red) mutations that confer FQ-resistance were generated via transformation followed by allelic replacement. Mutants were subjected to antimicrobial susceptibility testing for 12 clinically relevant antibiotics and ciprofloxacin. A decrease in MIC of each mutant relatively to that of the isogenic wild-type D39 strain (WT, green) was determined as collateral sensitivity (CS) and an increase as collateral resistance (CR). The growth rate of the WT and each mutant was determined to estimate *in vitro* fitness.

Figure 2. Collateral effect (CE) profiles for FQ-resistant *S. pneumoniae,* including *gyrA* (Mgx) and *parC* (Mpy) mutants, and *gyrA*::*parC* double mutants (Mgx::py). Antibiotics are ranked based on the hierarchical clustering of their associated collateral effects. Color indicates the magnitude of the collateral effect quantified as the mean log2 relative change of MIC compared to the WT. Red indicates collateral resistance (CR) and blue collateral sensitivity (CS).

Figure 3. Collateral effects (CE) are affected by epistatic interactions between *gyrA* and *parC* mutations in FQ-resistant *S. pneumoniae* mutants (Mgx::py). **A:** FQ-resistant strains (y-axis) and different antibiotics (x-axis) are hierarchically clustered based on their epistatic effects. Color intensity corresponds to the magnitude of epistasis, calculated using the additive model on a log-scale from the deviation

between the actual and the expected collateral effects of each double mutant (Mgx::py). Negative epistasis (blue) denotes a lower MIC of the double mutant than expected while positive epistasis (red) denotes a higher MIC than expected. Collateral resistance (CR) is indicated by an upwards triangle whereas collateral sensitivity (CS) with a downwards triangle. **B:** Relationship between epistasis and CE for each antibiotic. Black solid lines represent the linear regression of the epistasis-CE relationship for each antibiotic, where the magnitude of the effect size is represented by the steepness of the relationship. Due to the scarcity of Mgx::py mutants exhibiting CE the correlation for rifampicin (RIF) and vancomycin (VAN) could not be reliably estimated.

Figure 4. Fitness of FQ-resistant *S. pneumoniae* and correlation with epistatic and collateral effects (CE). **A:** Mean relative growth rate of three replicates of mutants harboring specific *gyrA* (gx) and/or *parC* (py) mutations. **B:** Relative growth rate of *gyrA* (Mgx, blue), *parC* (Mpy, orange), and *gyrA*::*parC* (Mgx::py, red) mutants compared to WT (green). Significant differences are indicated by * ($p<0.05$), ** ($p<0.01$), and *** ($p<0.001$).

Figure 5. Overview of treatment simulation workflow. **A**: Mutational trajectories used for simulations, with each trajectory consisting of four subpopulations representing the wild-type *S. pneumoniae* D39 (WT, green), a *gyrA* mutant (Mgx, blue), a *parC* mutant (Mpy, orange), and their corresponding *gyrA*::*parC* double mutant (Mgx::py, red). The experimentally determined MICs and relative growth rate (KG) for each specific strain were used to inform the model. **B:** Schematic of the stochastic hybrid ordinary deferential equation (ODE) model use for simulations. The

bacterial model comprised of ODEs describing the change of bacterial density over time for each subpopulation. Bacterial growth was modeled using a capacity limitation (G_{lim}) and a subpopulation specific growth rate ($k_{G,z}$). Unidirectional mutations were implemented as a stochastic event using random sampling from a binomial distribution with a probability representing the mutation frequency (μ) and sample size equal to the density of each bacterial subpopulation. The bacterial model was linked to a pharmacokinetic model of ciprofloxacin (CIP) and a pharmacokinetic model of erythromycin (ERY), linezolid (LNZ), or penicillin (PEN). Antibiotic effect ($E_{AB,z}$) was included on each subpopulation and was driven by the simulated plasma concentrations. If a combination treatment was simulated additivity was assumed. **C:** Treatments were simulated 1000 times per evolutionary trajectory. Pharmacokinetic profiles of an example combination treatment are depicted in the lower graph, while the nth realization of the bacterial dynamics corresponding to the example treatment are shown in the top graph. The probability of resistance (mutants) or failure of eradication (WT) was calculated for each evolutionary trajectory and treatment by summarizing the number of simulations for which bacterial concentrations exceeded the resistance cut-off (dashed line) at end of the treatment for each individual subpopulation.

Figure 6. Treatment outcomes of simulated clinical ciprofloxacin mono- or combination therapies. Each simulation includes WT (green), a *gyrA* mutant Mgx (blue), a *parC* mutant Mpy (orange), and the double mutant Mgx::py (red). **A**: Treatment outcomes of simulated clinical ciprofloxacin monotreatment (CIP, 500 mg b.i.d., average unbound steady state concentrations (C_{ss}) 1.39 mg/L) vary between different mutational trajectories (MTs). Solid line represents the median bacterial

growth dynamics of 1000 simulations where bacterial subpopulations are indicated by the respective color. The shaded areas represent the 5th and 95th simulated percentiles. The black dashed line represents the resistance cut-off, which is equal to the WT bacterial density at start of treatment. Although the bacterial dynamics and resistance development differed between the MTs, the simulated ciprofloxacin treatment was ineffective for all scenarios. **B:** End-of-treatment probability of resistance (mutants) and WT eradication failure, indicated in gray, were calculated for different MTs (panels), and subpopulations (x-axis) separately. **C:** Treatment outcome for clinical dosing regimens of ciprofloxacin monotreatment or combination therapies. Simulation outcomes with clinically relevant dosing regimens of ciprofloxacin as monotreatment and in combination with erythromycin (ERY, 600 mg b.i.d., C_{ss} 0.48 mg/L), linezolid (LNZ, 600 mg b.i.d., C_{ss} 7.33 mg/L), or penicillin (PEN, 3 g b.i.d., C_{ss} 6.95 mg/L). CIP as monotreatment had a high probably of resistance, foremost selecting for the *parC* mutant (Mpy, orange) and secondly the *gyrA* mutant (Mgx, blue). The addition of a second drug suppresses the probability of resistance for all treatments and evolutionary trajectories. All treatments eradicate the WT (green) and suppressed the double mutant (Mgx::py, red).

Figure 7. Treatment outcome of ciprofloxacin (CIP) monotreatment and in combination with erythromycin (ERY), linezolid (LNZ), or penicillin (PEN). The treatments were evaluated on eight different mutational trajectories to FQ resistance (see Figure 5A). **A:** Simulation outcomes of CIP in combination with ERY (top row panels), LNZ (mid row panels), or PEN (bottom row panels) with average unbound steady state concentrations (C_{ss}) around the MIC of the WT population (C_{ss} 0.25 - 2 x MIC). Concentration dependency related to WT strain eradication and resistance

evolution. **B:** End-of-treatment probability of resistance (mutants) and treatment failure (WT) for antibiotic doses resulting in an average steady state plasma concentration of CIP and LNZ equal to the 0.5 x MIC of the WT. Collateral effects (CE) are indicated by the color of text, where blue represents collateral sensitivity (CS), black no CE, red collateral resistance (CR), and gray when CE is not applicable (NA). The mutational trajectory, *i.e.* the multistep alternative pathways for the *de novo* emergence of a particular high-level FQ-resistant double mutant (Mgx::py), had an impact on treatment outcome, although it was not the sole determinant.

Figure 8. Relationship between collateral effect, relative growth rate, and probability of resistance under antibiotic combinations. Simulation of the eight defined *S. pneumoniae* mutational trajectories (indicated by number) treated with a combination ciprofloxacin and penicillin (PEN) with average steady state plasma concentrations equal to the 0.5 x MIC the WT. The collateral effect (CE) of PEN is represented on the x-axis and the probability of resistance at the end of treatment on the y-axis. Colors indicate the relative growth rate of each mutant compared to the WT. Each panel column denotes a FQ-resistant mutant subpopulation (Mgx, Mpy or Mgx::py) with the top panels representing simulations were no collateral or fitness effects were included, top mid panels based solely on the experimentally determined relative growth rate, lower mid panels based solely on the experimentally determined collateral effects, and the lower panel based both on the collateral and fitness effects.

Figure S1. Ciprofloxacin MICs for the wild-type *S. pneumoniae* D39 (WT, green), gyrA mutants (Mgx, blue), parC mutants (Mpy, orange), and their corresponding gyrA::parC double mutant (Mgx::py, red).

Figure S2. Hierarchical clustering based on collateral effects between strains and antibiotics. Collateral effect for FQ-resistant strains (y axis) against different antibiotics (x-axis). Color intensity corresponds to the collateral effect magnitude quantified by the mean log2 relative change of MIC compared to the WT. Collateral resistance (CR) and collateral sensitivity (CS) are respectively depicted with red and blue.

Figure S3. Epistastic effects of FQ-resistance mutations on fitness of Mgx::py mutants. Color intensity corresponds to the magnitude of epistatic effects, calculated using the additive model from the deviation between the actual and the expected growth rate value of each double mutant (Mgx::py). Negative epistasis (blue) denotes a lower growth rate and higher fitness cost of the double mutant than expected while positive epistasis (red) denotes a higher growth rate and lower fitness cost than expected.

Figure S4. Correlation between mean relative growth rate (KG) and collateral effect (CE). Mean relative growth rate of mutants harboring specific *gyrA* (gx) and/or *parC* (py) mutations compared to WT versus CE, where red indicate collateral resistance (CR), black no CE, and blue collateral sensitivity (CS).

Figure S5. Overall bacterial dynamics of simulated ciprofloxacin mono- or combination with erythromycin (ERY), linezolid (LNZ), or penicillin (PEN). Each simulation includes WT (green), a *gyrA* mutant Mgx (blue), a *parC* mutant Mpy (orange), and the double mutant Mgx::py (red). Simulation outcomes treated with CIP

in combination with ERY, LNZ, or PEN with average unbound steady state concentrations (C_{ss}) around the MIC of the WT population (C_{ss} 0.25 - 2 x MIC). The treatments were evaluated on eight different mutational trajectories to FQ resistance (see Figure 5A). Solid line represents the median bacterial growth dynamics of 1000 simulations where bacterial subpopulations are indicated by the respective color. The shaded areas represent the 5th and 95th simulated percentiles. The black dashed line represents the resistance cut-off, which is equal to the WT bacterial density at start of treatment.

Figure S6. Overall treatment outcomes of simulated ciprofloxacin mono- or combination with erythromycin (ERY), linezolid (LNZ), or penicillin (PEN). Simulation outcomes treated with CIP in combination with ERY, LNZ, or PEN with average unbound steady state concentrations (C_{ss}) around the MIC of the WT population (C_{ss} 0.25 - 2 x MIC). Mutant subpopulations included a *gyrA* mutant Mgx, a *parC* mutant Mpy, and the double mutant Mgx::py. The treatments were evaluated on eight different mutational trajectories to FQ resistance. End-of-treatment probability of resistance (mutants) and treatment failure (WT), indicated in gray, were calculated for the different treatments (panels), mutational trajectories (y-axis), and subpopulations (x-axis) separately. Collateral effects (CE) are indicated in color of text, where blue represents collateral sensitivity (CS), black no CE, red collateral resistance (CR), and dark green when CE is not applicable (NA).

Figure S7. Relationship between collateral effect, relative growth rate, and probability of resistance under antibiotic combination with different strength of selective pressure. Simulation of the eight defined *S. pneumoniae* mutational

trajectories (indicated by number) treated with a combination ciprofloxacin and linezolid (LNZ) with average steady state plasma concentrations equal to the 1 x MIC and 0.25 x MIC of the WT, respectively. The collateral effect (CE) of LNZ is represented on the x-axis and the probability of resistance at end of treatment on the y-axis. Color indicate the relative growth rate of each mutant compared to the WT. Each panel column denotes a FQ-resistant mutant subpopulation (Mgx, Mpy or Mgx::py) with the top panels representing simulations were no collateral or fitness effects were included, top mid panels based solely on the experimentally determined relative growth rate, lower mid panels based solely on the experimentally determined collateral effects, and the lower panel based both on the collateral and fitness effects.

Appendix 1.

Ordinary differential equation (ODE) system

$$A_{CIP}[k+1] = -k_{e,CIP} \times A_{CIP}[k]$$
$$C_{CIP}[k] = \frac{A_{CIP}[k]}{V_{CIP}}$$

If AB = LNZ or PEN

$$A_{AB}[k+1] = -k_{e,AB} \times A_{AB}[k]$$

If AB = ERY

$$A_{AB}[k+1] = -k_{e,AB} \times A_{AB}[k] - k_{12,AB} \times A_{AB}[k] + k_{21,AB} \times A_{AB,P}[k]$$
$$A_{AB,P}[k+1] = k_{12,AB} \times A_{AB}[k] - k_{21,AB} \times A_{AB,P}[k]$$

$$C_{AB}[k] = \frac{A_{AB}[k]}{V_{AB}}$$

$$WT[k+1] = WT[k] \times \left(1 - \frac{WT[k]+Mgx[k]+Mpy[k]+Mgx{::}py[k]}{B_{max}}\right) \times k_{G,WT} \times \left(1 - \left(\frac{\left(G_{max}-G_{min,CIP}\right)\times\left(\frac{C_{CIP}[k]}{MIC_{CIP,WT}}\right)^{hill_{CIP}}}{\left(\frac{C_{CIP}[k]}{MIC_{CIP,WT}}\right)^{hill_{CIP}} - \frac{G_{min,CIP}}{G_{max}}} + \frac{\left(G_{max}-G_{min,AB}\right)\times\left(\frac{C_{AB}[k]}{MIC_{AB,WT}}\right)^{hill_{AB}}}{\left(\frac{C_{AB}[k]}{MIC_{AB,WT}}\right)^{hill_{CIP}} - \frac{G_{min,AB}}{G_{max}}} + \right)\right) - k_{WT,Mgx} - k_{WT,Mpy} - k_e \times WT[k]$$

$$Mgx[k+1] = Mgx[k] \times \left(1 - \frac{WT[k]+Mgx[k]+Mpy[k]+Mgx{::}py[k]}{B_{max}}\right) \times k_{G,Mgx} \times \left(1 - \left(\frac{\left(G_{max}-G_{min,CIP}\right)\times\left(\frac{C_{CIP}[k]}{MIC_{CIP,Mgx}}\right)^{hill_{CIP}}}{\left(\frac{C_{CIP}[k]}{MIC_{CIP,Mgx}}\right)^{hill_{CIP}} - \frac{G_{min,CIP}}{G_{max}}} + \frac{\left(G_{max}-G_{min,AB}\right)\times\left(\frac{C_{AB}[k]}{MIC_{AB,Mgx}}\right)^{hill_{AB}}}{\left(\frac{C_{AB}[k]}{MIC_{AB,Mgx}}\right)^{hill_{CIP}} - \frac{G_{min,AB}}{G_{max}}} + \right)\right) + k_{WT,Mgx} - k_{Mgx,Mgx{::}py} - k_e \times Mgx[k]$$

$$Mpy[k+1] = Mpy[k] \times \left(1 - \frac{WT[k]+Mgx[k]+Mpy[k]+Mgx{::}py[k]}{B_{max}}\right) \times k_{G,Mpy} \times \left(1 - \left(\frac{\left(G_{max}-G_{min,CIP}\right)\times\left(\frac{C_{CIP}[k]}{MIC_{CIP,Mpy}}\right)^{hill_{CIP}}}{\left(\frac{C_{CIP}[k]}{MIC_{CIP,Mpy}}\right)^{hill_{CIP}} - \frac{G_{min,CIP}}{G_{max}}} + \frac{\left(G_{max}-G_{min,AB}\right)\times\left(\frac{C_{AB}[k]}{MIC_{AB,Mpy}}\right)^{hill_{AB}}}{\left(\frac{C_{AB}[k]}{MIC_{AB,Mpy}}\right)^{hill_{CIP}} - \frac{G_{min,AB}}{G_{max}}} + \right)\right) + k_{WT,Mpy} - k_{Mpy,Mgx{::}py} - k_e \times Mpy[k]$$

$$Mgx{:}\,py[k+1] = Mgx{:}\,py[k] \times \left(1 - \frac{WT[k]+Mgx[k]+Mpy[k]+Mgx{:}py[k]}{B_{max}}\right) \times k_{G,Mgx{::}py} \times \left(1 - \left(\frac{\left(G_{max}-G_{min,CIP}\right)\times\left(\frac{C_{CIP}[k]}{MIC_{CIP,Mgx{::}py}}\right)^{hill_{CIP}}}{\left(\frac{C_{CIP}[k]}{MIC_{CIP,Mgx{::}py}}\right)^{hill_{CIP}} - \frac{G_{min,CIP}}{G_{max}}} + \frac{\left(G_{max}-G_{min,AB}\right)\times\left(\frac{C_{AB}[k]}{MIC_{AB,Mgx{::}py}}\right)^{hill_{AB}}}{\left(\frac{C_{AB}[k]}{MIC_{AB,Mgx{::}py}}\right)^{hill_{CIP}} - \frac{G_{min,AB}}{G_{max}}} + \right)\right) + k_{Mgx,Mgx{::}py} + k_{Mpy,Mgx{::}py} - k_e \times Mgx{:}\,py[k]$$

$k = 0,1, 2 \ldots 324$

$$k_{WT,Mgx} = \frac{Pr(\kappa_{WT,Mgx}; WT[k], \mu)}{V}$$

$\kappa_{WT,Mgx} = 0,1,2 \ldots WT[k]$

$$k_{WT,Mpy} = \frac{Pr(\kappa_{WT,Mpy}; WT[k], \mu)}{V}$$

$\kappa_{WT,Mpy} = 0,1,2 \ldots WT[k]$

$$k_{Mgx,Mgx::py} = \frac{Pr(\kappa_{Mgx}; Mgx[k], \mu)}{V}$$

$\kappa_{Mgx} = 0,1,2 \ldots Mgx[k]$

$$k_{Mpy,Mgx::py} = \frac{Pr(\kappa_{Mpy}; Mpy[k], \mu)}{V}$$

$\kappa_{Mpy} = 0,1,2 \ldots Mpy[k]$

Appendix 2.

Derived concentration-effect relationships

We digitized early phase data (≤ 6 h after start of experiment) from previously performed *in vitro* static time-kill experiments treating *S. pneumoniae* with ciprofloxacin, erythromycin, linezolid, or penicillin. Summary of the collected data can be found in **Table A2.1**. The data was subsequently used for fitting antibiotic specific pharmacodynamic models. All fitted models could satisfactory describe the observed data (**Figure A2.1**). Penicillin was estimated to have the largest maximal drug effect (E_{max} = 2.64) and linezolid the lowest (E_{max} = 1.53), while small between antibiotic differences were seen for the Hill factor (range 2.7-2.99) (**Table A2.2**, **Figure A2.2**).

Table A2.1. Overview of collected litterateur data of *in vitro* time-kill studies on *S. pneumoniae*.

Drug	Concentration range	N conc	MIC	ID	Reference
CIP	0.125-16 μg/mL	8	2.0 μg/mL	1	(28)
CIP	0.25-32 μg/mL	8	4.0 μg/mL	2	(28)
CIP	0.25-32 μg/mL	8	4.0 μg/mL	3	(28)
CIP	0.125-16.0 μg/mL	8	2.0 μg/mL	4	(29)
CIP	0.002-0.064 μg/mL	5	0.008 μg/mL	5	(30)
ERY	0.004-0.5 μg/mL	8	0.06 μg/mL	1	(28)
ERY	2-256 μg/mL	8	32 μg/mL	2	(28)
ERY	0.5-64 μg/mL	8	8.0 μg/mL	3	(28)
ERY	0.05-0.4 μg/mL	3	0.1 μg/mL	4	(31)
LNZ	1.0-20 μg/mL	4	1.0 μg/mL	1	(32)
PEN	0.001-0.125 μg/mL	9	0.015 μg/mL	1	(28)
PEN	0.015-2.0 μg/mL	9	0.25 μg/mL	2	(28)
PEN	0.125-16.0 μg/mL	9	2.0 μg/mL	3	(28)
PEN	0.250-32.0 μg/mL	9	4.0 μg/mL	4	(29)
PEN	4 – 32 μg/mL	4	8.0 μg/mL	5	(33)
PEN	0.008-0.064 μg/mL	4	0.016 μg/mL	6	(33)

Drug	$\mathbf{E_{max}}$ (95%CI) [RSE%]	**Hill factor** (95%CI) [RSE%]
Ciprofloxacin	1.96 (1.86-2.7) [4.17]	2.8 (2.2-3.56) [11.9]
Erythromycin	1.64 (1.51-1.79 [8.79]	2.85 (1.97-4.13) [18]
Linezolid	1.53 (1.47-1.6) [5.07]	2.99 (0.041-217) [200]
Penicillin	2.64 (2.46-2.83) [3.66]	2.7 (2.1-3.47) [12.9]

Table A2.2. Pharmacodynamic model parameters.

CI confidents interval, RSE relative standard error

Figure A2.1. Predicted (lines) and observed (points) bacterial densities of *S. pneumoniae* treated with ciprofloxacin (CIP), erythromycin (ERY), linezolid (LIN), penicillin (PEN), where color indicate antibiotic concentration normalized over the MIC.

Figure A2.2. Pharmacodynamic concentration effect relationship of ciprofloxacin (CIP), erythromycin (ERY), linezolid (LIN), penicillin (PEN).

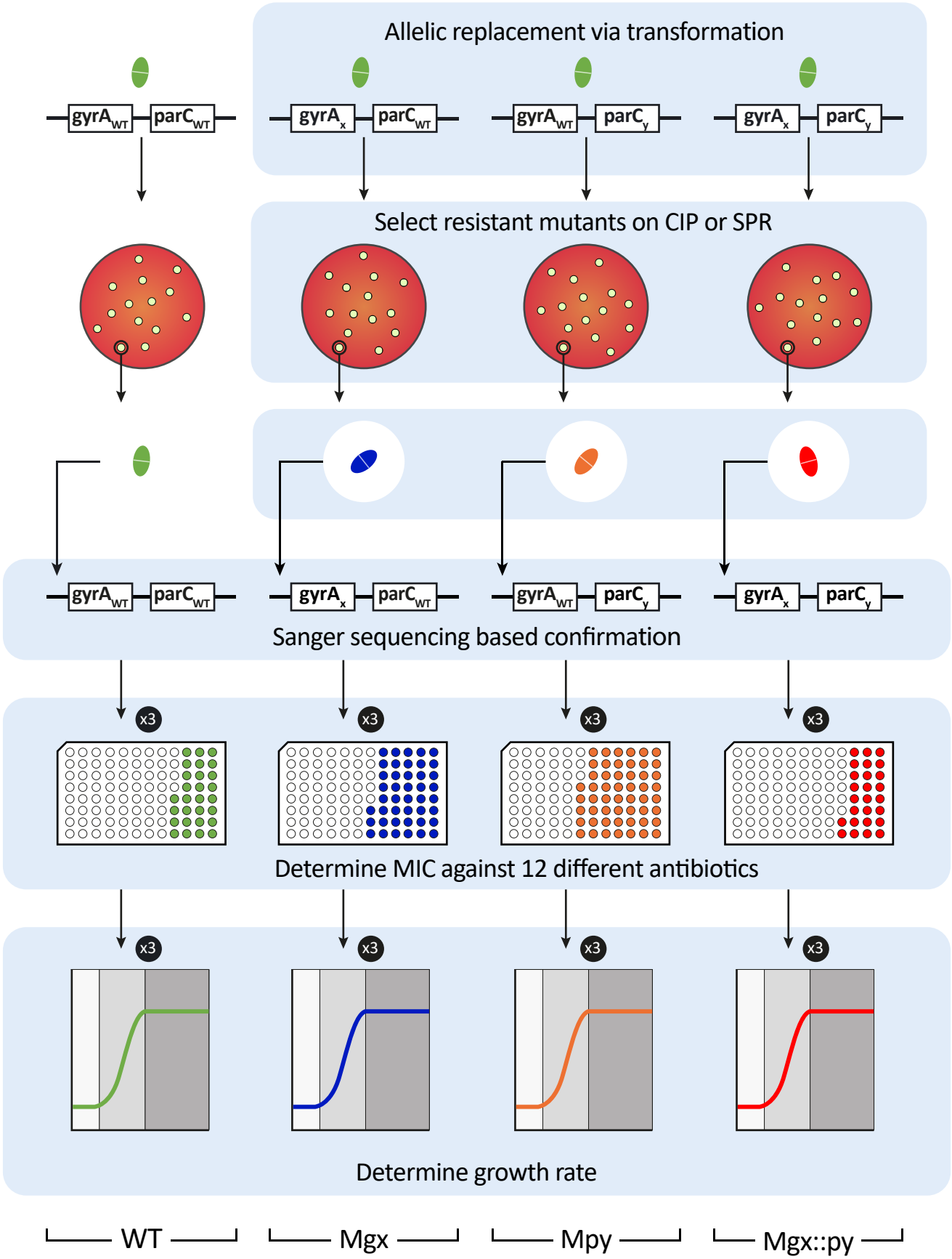
Allelic replacement via transformation
gyrA_WT
parC_WT
gyrA_x
parC_WT
gyrA_WT
parC_y
gyrA_x
parC_y
Select resistant mutants on CIP or SPR
Sanger sequencing based confirmation
x3
Determine MIC against 12 different antibiotics
Determine growth rate
WT
Mgx
Mpy
Mgx::py

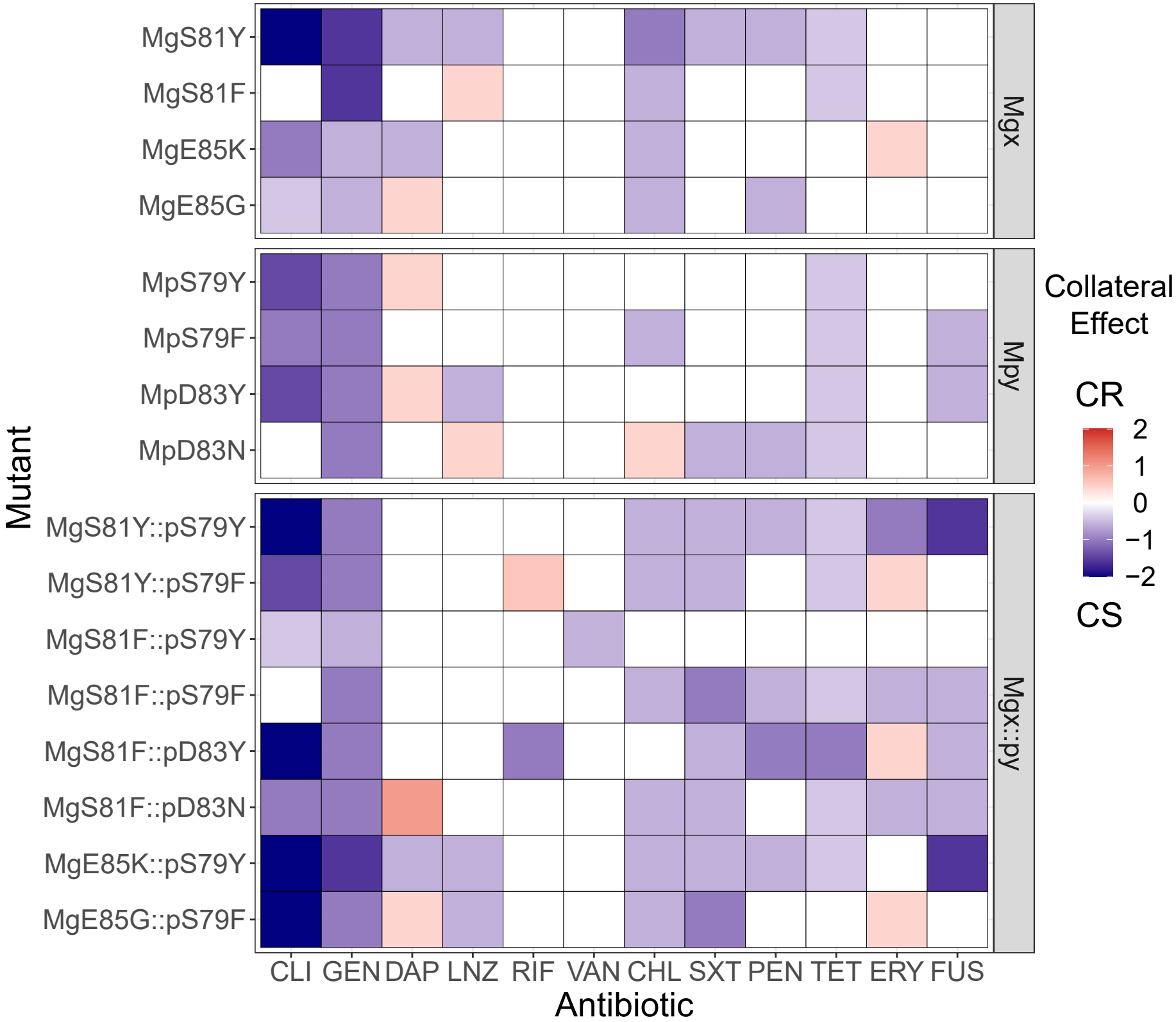
Mgx
Mpy
Mgx::py
MgS81Y
MgS81F
MgE85K
MgE85G
MpS79Y
MpS79F
MpD83Y
MpD83N
MgS81Y::pS79Y
MgS81Y::pS79F
MgS81F::pS79Y
MgS81F::pS79F
MgS81F::pD83Y
MgS81F::pD83N
MgE85K::pS79Y
MgE85G::pS79F
Mutant
CLI GEN DAP LNZ RIF VAN CHL SXT PEN TET ERY FUS
Antibiotic
Collateral Effect
CR
2
1
0
−1
−2
CS

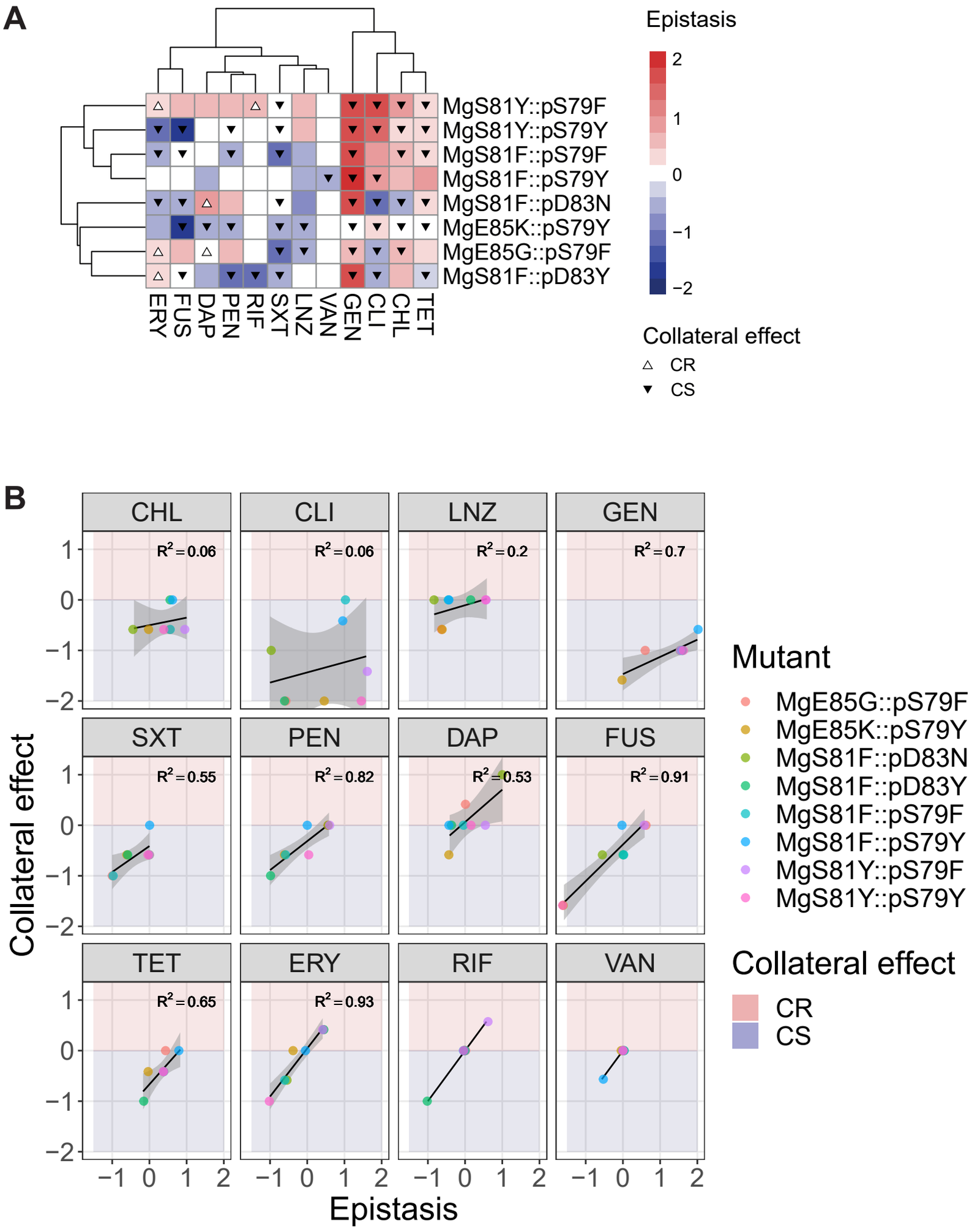
A
Epistasis
2
1
0
−1
−2
MgS81Y::pS79F
MgS81Y::pS79Y
MgS81F::pS79F
MgS81F::pS79Y
MgS81F::pD83N
MgE85K::pS79Y
MgE85G::pS79F
MgS81F::pD83Y
ERY
FUS
DAP
PEN
RIF
SXT
LNZ
VAN
GEN
CLI
CHL
TET
Collateral effect
CR
CS
B
CHL
CLI
LNZ
GEN
SXT
PEN
DAP
FUS
TET
ERY
RIF
VAN
R² = 0.06
R² = 0.06
R² = 0.2
R² = 0.7
R² = 0.55
R² = 0.82
R² = 0.53
R² = 0.91
R² = 0.65
R² = 0.93
Collateral effect
Epistasis
Mutant
MgE85G::pS79F
MgE85K::pS79Y
MgS81F::pD83N
MgS81F::pD83Y
MgS81F::pS79F
MgS81F::pS79Y
MgS81Y::pS79F
MgS81Y::pS79Y
Collateral effect
CR
CS

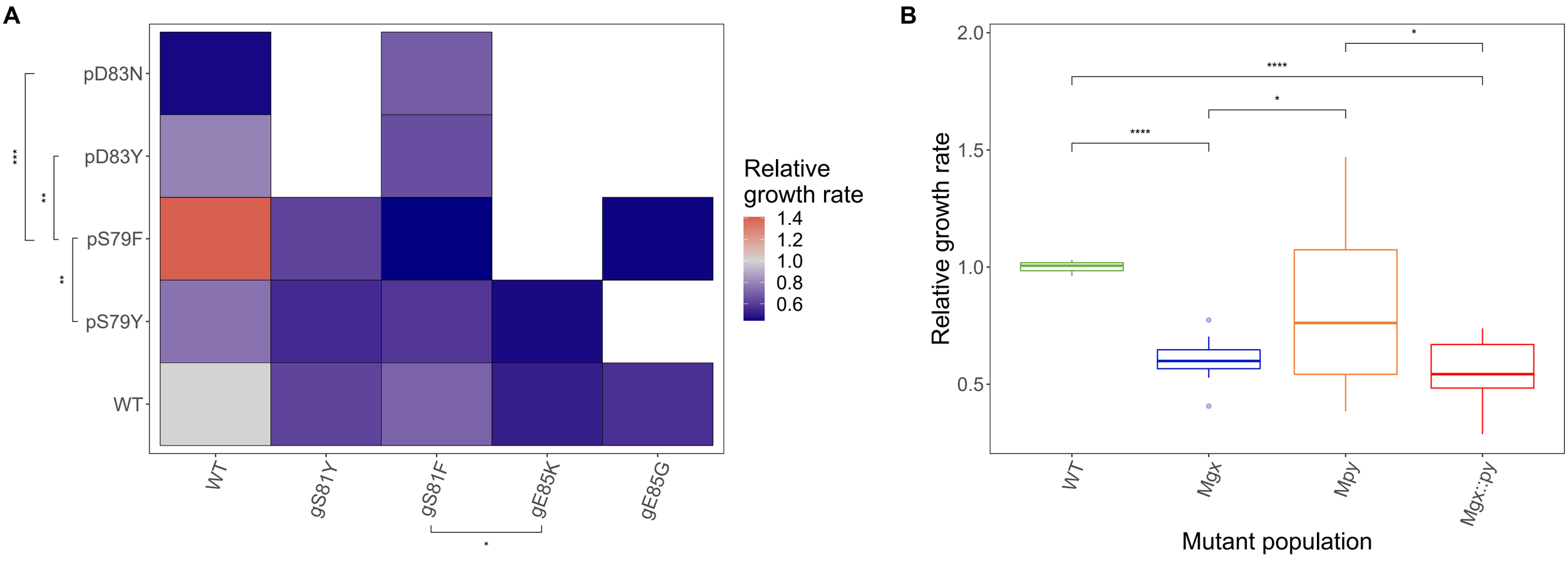
A
pD83N
pD83Y
pS79F
pS79Y
WT
WT
gS81Y
gS81F
gE85K
gE85G
***
**
**
*
Relative growth rate
1.4
1.2
1.0
0.8
0.6
B
Relative growth rate
2.0
1.5
1.0
0.5
****
*
****
*
WT
Mgx
Mpy
Mgx::py
Mutant population

A

Mutational trajectory	WT	Mgx	Mpy	Mgx::py
1	$gyrA_{wt}$:$parC_{wt}$	$gyrA_{S81F}$:$parC_{wt}$	$gyrA_{wt}$:$parC_{D83N}$	$gyrA_{S81F}$:$parC_{D83N}$
2	$gyrA_{wt}$:$parC_{wt}$	$gyrA_{S81F}$:$parC_{wt}$	$gyrA_{wt}$:$parC_{D83Y}$	$gyrA_{S81F}$:$parC_{D83Y}$
3	$gyrA_{wt}$:$parC_{wt}$	$gyrA_{E85G}$:$parC_{wt}$	$gyrA_{wt}$:$parC_{S79F}$	$gyrA_{E85G}$:$parC_{S79F}$
4	$gyrA_{wt}$:$parC_{wt}$	$gyrA_{S81F}$:$parC_{wt}$	$gyrA_{wt}$:$parC_{S79F}$	$gyrA_{S81F}$:$parC_{S79F}$
5	$gyrA_{wt}$:$parC_{wt}$	$gyrA_{S81Y}$:$parC_{wt}$	$gyrA_{wt}$:$parC_{S79F}$	$gyrA_{S81Y}$:$parC_{S79F}$
6	$gyrA_{wt}$:$parC_{wt}$	$gyrA_{E85K}$:$parC_{wt}$	$gyrA_{wt}$:$parC_{S79Y}$	$gyrA_{E85K}$:$parC_{S79Y}$
7	$gyrA_{wt}$:$parC_{wt}$	$gyrA_{S81F}$:$parC_{wt}$	$gyrA_{wt}$:$parC_{S79Y}$	$gyrA_{S81F}$:$parC_{S79Y}$
8	$gyrA_{wt}$:$parC_{wt}$	$gyrA_{S81Y}$:$parC_{wt}$	$gyrA_{wt}$:$parC_{S79Y}$	$gyrA_{S81Y}$:$parC_{S79Y}$

B

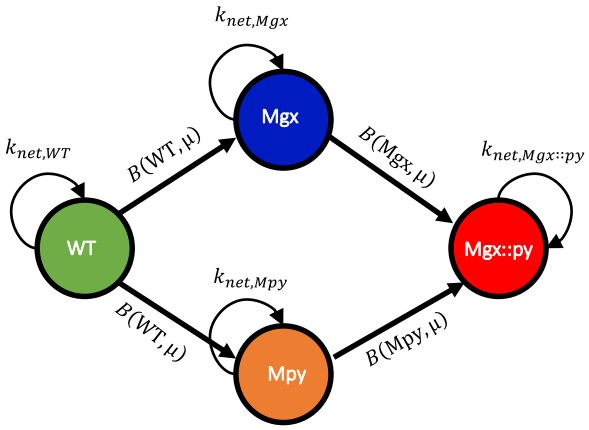

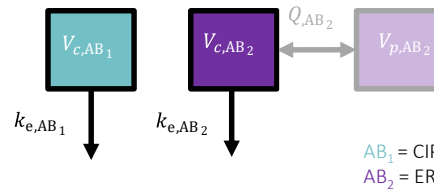

Bacterial dynamics: $k_{net,z} = k_{G,z} \times G_{lim} \times E_{AB,z}$

Growth limitation: $G_{lim} = 1 - \frac{\mathrm{WT} + \mathrm{Mgx} + \mathrm{Mpy} + \mathrm{Mgx::py}}{10^{B_{max}}}$

Antibiotic effect: $E_{AB,z} = \prod_{i=1}^{n} E_{AB,i,z}(C_{AB,i}, MIC_{ABi,z}, G_{min,AB,i}, hill_{AB,i})$

n = 1 → Mono-treatment
n = 2 → Combination treatment

C

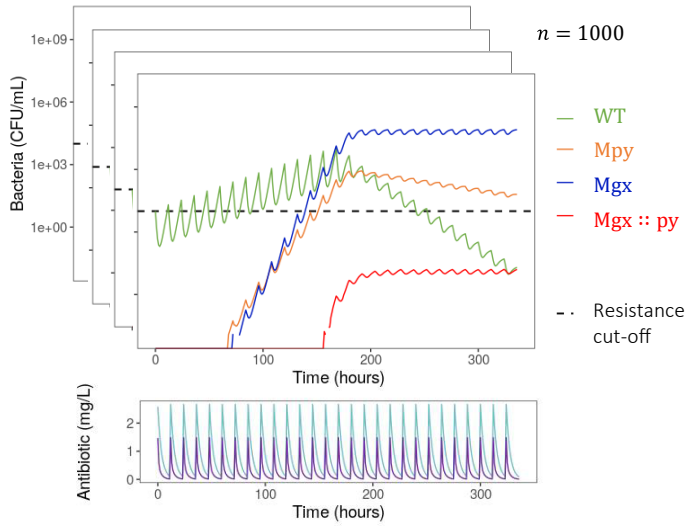

Probability of resistance and WT eradication failure:

At end of treatment:

$$P_{R,M_x} = \frac{\sigma_1^n \mathrm{M}_{x,i} > \text{cut-off}_{\text{resistance}}}{n} \times 100$$

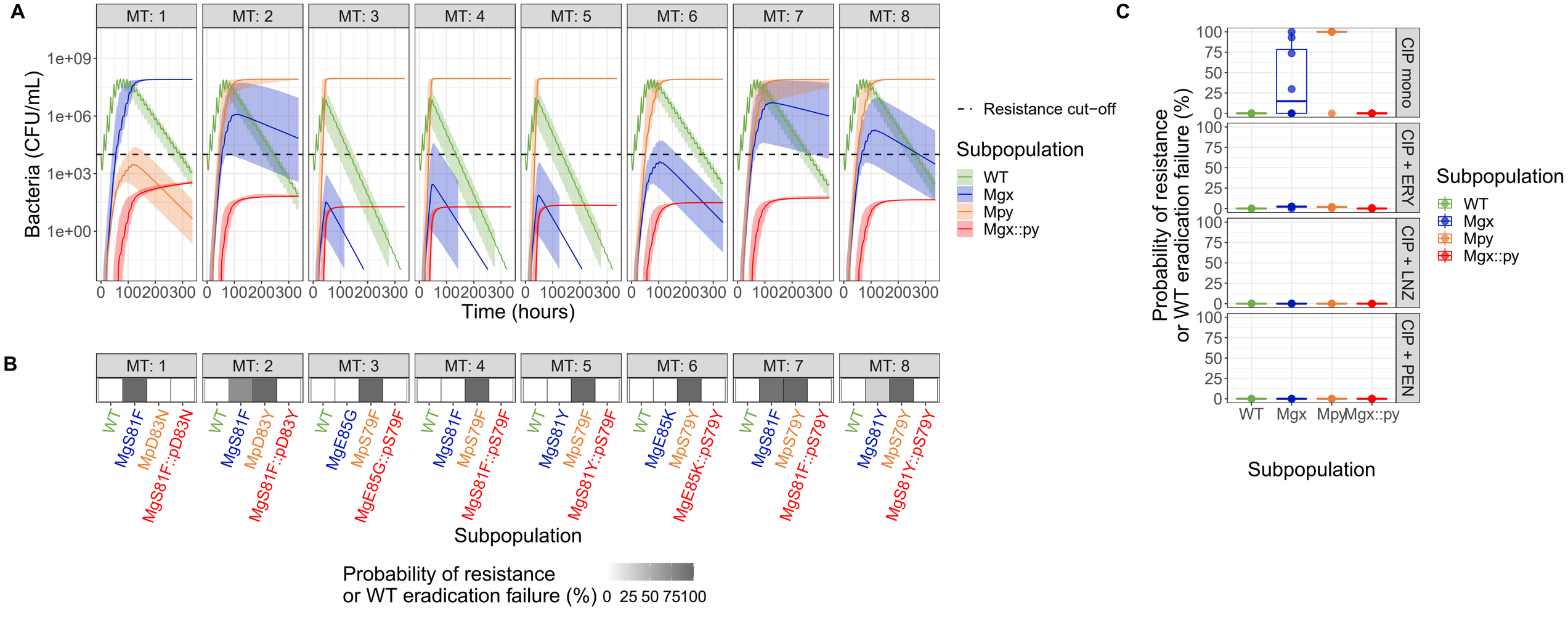
A
MT: 1
MT: 2
MT: 3
MT: 4
MT: 5
MT: 6
MT: 7
MT: 8
Bacteria (CFU/mL)
1e+09
1e+06
1e+03
1e+00
0 100200300
Time (hours)
Resistance cut−off
Subpopulation
WT
Mgx
Mpy
Mgx::py
B
WT
MgS81F
MpD83N
MgS81F::pD83N
MpD83Y
MgS81F::pD83Y
MgE85G
MpS79F
MgE85G::pS79F
MgS81F::pS79F
MgS81Y
MgS81Y::pS79F
MgE85K
MgE85K::pS79Y
Subpopulation
Probability of resistance
or WT eradication failure (%) 0 25 50 75100
C
Probability of resistance
or WT eradication failure (%)
CIP mono
CIP + ERY
CIP + LNZ
CIP + PEN
WT
Mgx
Mpy
Mgx::py
Subpopulation

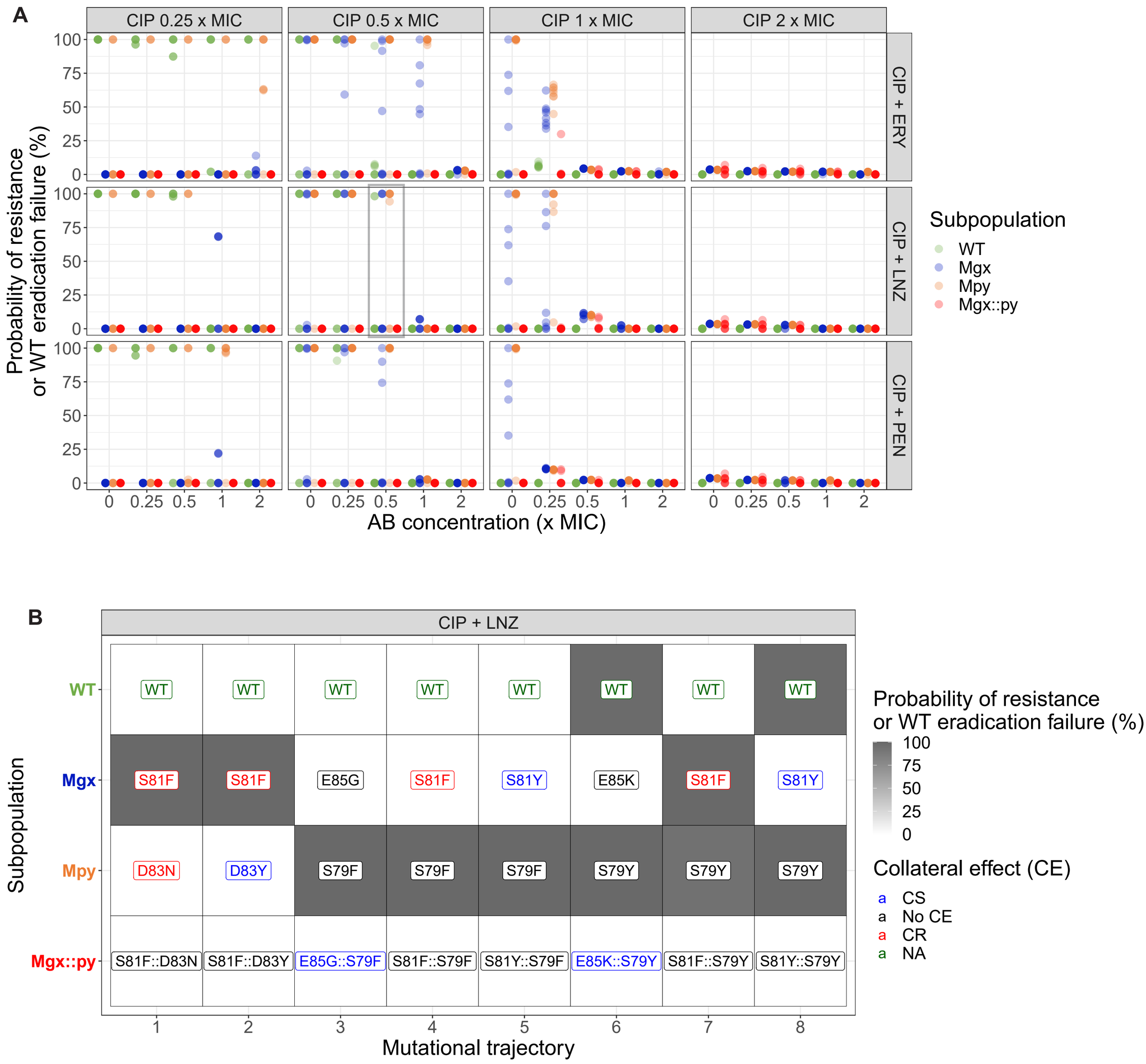
A
CIP 0.25 x MIC
CIP 0.5 x MIC
CIP 1 x MIC
CIP 2 x MIC
CIP + ERY
CIP + LNZ
CIP + PEN
Probability of resistance or WT eradication failure (%)
100
75
50
25
0
0
0.25
0.5
1
2
AB concentration (x MIC)
Subpopulation
WT
Mgx
Mpy
Mgx::py
B
CIP + LNZ
WT
Mgx
Mpy
Mgx::py
Subpopulation
WT WT WT WT WT WT WT WT
S81F S81F E85G S81F S81Y E85K S81F S81Y
D83N D83Y S79F S79F S79F S79Y S79Y S79Y
S81F::D83N S81F::D83Y E85G::S79F S81F::S79F S81Y::S79F E85K::S79Y S81F::S79Y S81Y::S79Y
1
2
3
4
5
6
7
8
Mutational trajectory
Probability of resistance or WT eradication failure (%)
100
75
50
25
0
Collateral effect (CE)
a CS
a No CE
a CR
a NA

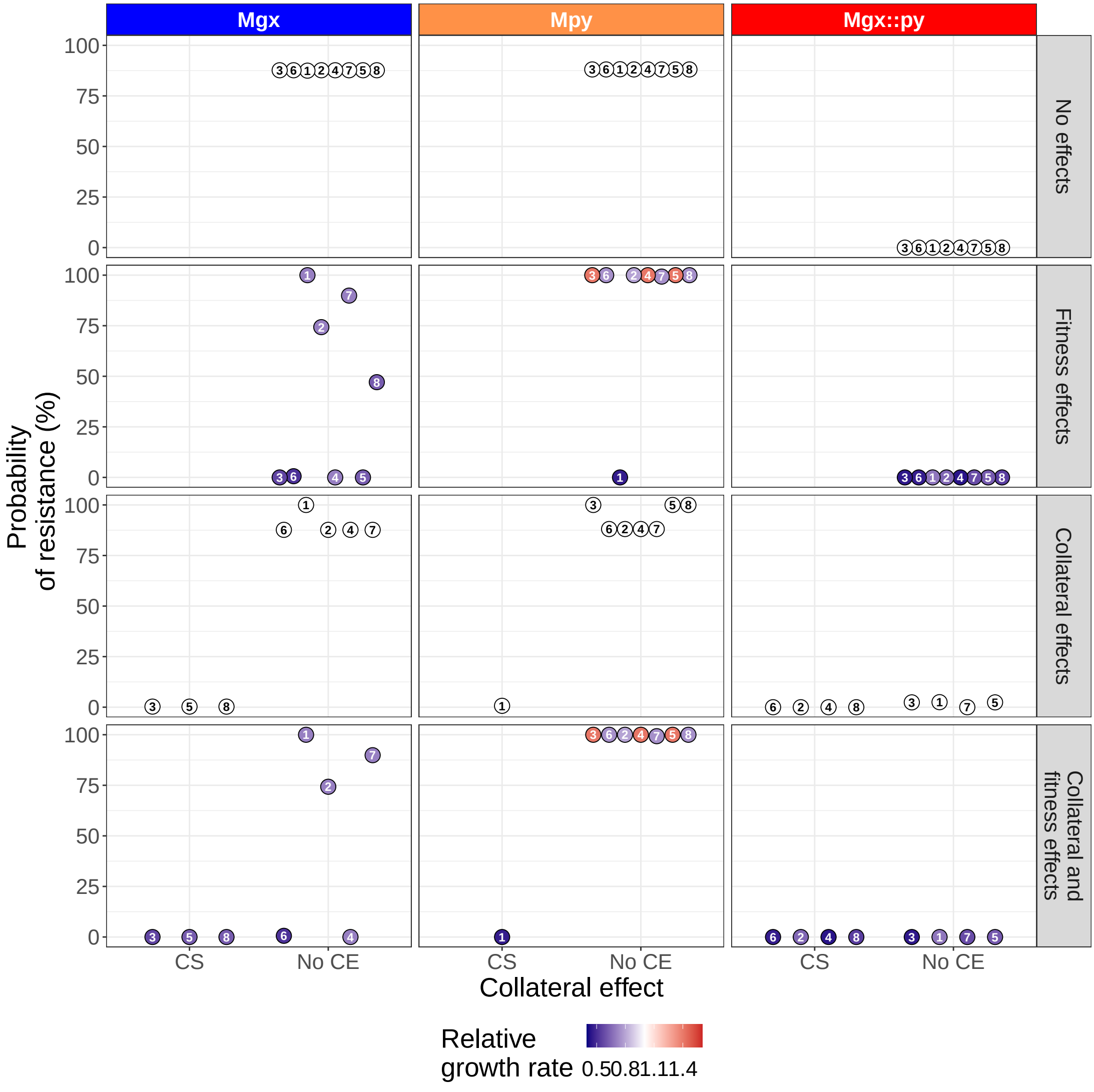
Mgx
Mpy
Mgx::py
No effects
Fitness effects
Collateral effects
Collateral and fitness effects
Probability of resistance (%)
100
75
50
25
0
CS
No CE
Collateral effect
Relative growth rate
0.5
0.8
1
1.1
4